Progress in Particle and Nuclear Physics 63 (2009) 155–185

Contents lists available at ScienceDirect

Progress in Particle and Nuclear Physics

journal homepage: www.elsevier.com/locate/ppnp

Review

Fission times of excited nuclei: An experimental overview

D. Jacquet [a], M. Morjean [b,*]

[a] IPNO, CNRS/IN2P3, Université Paris-Sud 11, F-91406 Orsay Cedex, France
[b] GANIL, CEA-DSM and IN2P3-CNRS, B.P. 55027, F-14076 Caen Cedex, France

ARTICLE INFO

Keywords:
Fission
Fission time
Nuclear dissipation
Friction
Super-heavy nuclei

ABSTRACT

An overview of selected recent experimental results on fission times is presented. Evidences for over-damped motion up to saddle point during the fission process of highly excited nuclei have been obtained independently through fission probability, pre-scission multiplicity and direct time measurements. In addition, strong clues have been found for a temperature dependency of friction. Experiments probing transient effects through fission probabilities are presented and the counterbalanced effects of friction and level density parameters are discussed. Promising perspectives for super-heavy stability studies, based on fission time measurements, are presented.

Contents

1. Introduction

Fission is a dynamical process for which a nucleus needs time to deform up to scission. Since the discovery of fission by Hahn and Strassmann [1], important theoretical and experimental efforts have been undertaken to determine this time and its various components associated with the different steps of the process. Nevertheless, due to the complexity of the process and to the restricted time ranges covered by the clocks used experimentally, quite different time scales have been reached, leading to quite different views of the collective motion of the nucleons for small and large deformations of the nuclei.

Immediately after the discovery of fission, Bohr and Wheeler in a famous paper [2] proposed a model that nowadays still guides most of our understanding of the process. Fission was treated as a diffusion process over a potential barrier in which

* Corresponding author. Tel.: +33 2 31 45 45 04; fax: +33 2 31 45 46 65.
E-mail address: morjean@ganil.fr (M. Morjean).

0146-6410/$ – see front matter © 2008 Elsevier B.V. All rights reserved.
doi:10.1016/j.ppnp.2008.10.001

the nucleus is trapped at the beginning inside a potential pocket. The nucleus can however escape the pocket through a saddle point beyond which it is inevitably driven by the potential towards scission into two fission fragments. During the whole process, the system can cool down by particle emission and therefore, the mass, the temperature as well as the fission barrier are modified. In order to include light particle evaporation and fission within a unique statistical approach, the transition state theory was applied to fission in the Bohr and Wheeler model. A fission rate R^{BW} was calculated from the flux from inside to outside the saddle point, considered as a transition state. A statistical fission width $\Gamma^{BW} = \hbar \times R^{BW}$ was then inferred and the Weisskopf formalism was extended to include competition between fission and particle evaporation, giving access to the fission probability. The time for the whole fission process in this approach is thus simply given by the fission rate and by the dynamical evolution between the saddle and scission points. However, in a general paper on friction effects published in 1940, Kramers [3] stressed, from a solution of the Fokker–Plank equation applied to fission, that if the nuclear matter has a high viscosity, the fission rates as calculated within the Bohr and Wheeler approach are too high: dissipation of collective modes to intrinsic ones slows down the motion and the resulting fluctuating force can bring nuclei back inside the saddle point with a non-negligible probability.

The Bohr and Wheeler model, ignoring possible friction effects, was quite successfully applied until it failed in reproducing the first data on pre-scission neutron multiplicities obtained by Gavron [4,5]. This failure was then interpreted [6,7] as an evidence for friction effects, slowing down the fission process and thus leading to higher pre-scission particle multiplicities than predicted by the Bohr and Wheeler model. Following this conclusion, the Kramers formulation has been frequently included in statistical models of fission. However, more recent data and analyses that will be presented in this paper shed doubts on this conclusion since they conclude that a large part of the pre-scission emission takes place between the saddle and scission points. The necessity to consider friction effects as well as the time scales of the process are thus still nowadays under debate.

A review of the first efforts in order to determine fission time scales has been made in 1992 by Hilscher and Rossner [8]. Since this review, important progresses have been made in the experimental approaches, in the data analyses and interpretations, leading to more reliable conclusions. In the present paper, we shall focus on these new results. They are often inferred from statistical models in which dynamical effects are sometimes considered and mocked-up following different prescriptions in order to get insights into the magnitude of friction effects. However, the dynamical evolution of the fissioning system also depends on the considered potential energy landscape, inertia, collective excitations…that are taken into account through many parameters and more or less arbitrary assumptions differing with the considered model. A reliable evaluation of the numerous existing models would require comparing their predictions to a unique set of representative data, an issue clearly out of the scope of the present experimental overview. For each of the models we shall only give a short presentation underlining its originality and refer the reader to the most relevant published references for further details. However, we shall stress in each case the main hypotheses done on the parameter values or on the underlying mechanisms and the resulting uncertainties on the conclusions. We shall finally point out the common conclusions that do not depend on the considered models as well as those obtained from direct experimental approaches that do not involve any nuclear model.

In Section 2, the various time scales playing a role in the fission process will be described and the new data and conclusions concerning friction effects will be presented in Sections 3.1 and 4. In Section 3.2, quite promising results of recent experiments probing the stability of super-heavy elements through their fission times will be presented.

2. Different times involved during the fission process

The total time involved in a fission process can be schematically divided in two main components, assuming as a starting point a fully equilibrated nucleus. The first component corresponds to the time needed by the nucleus to pass irrevocably over the saddle point. At this time, fission is decided and the nucleus inevitably deforms toward scission. The second component corresponds to the deformation time from the saddle up to the scission point. The acceleration time of the fission fragments after scission is very short and can be neglected, whereas the much longer de-excitation time of the fission fragments after scission, leading to post-scission emission, does not bring any further information on the process and will not be considered in the following. Such a division in two main components is however somewhat arbitrary since the dynamical evolution of the nucleus is always essentially governed by the potential and the temperature.

In addition to the two main components that will be more precisely defined in the following subsections, other time scales have always to be considered, making the fission process quite difficult to simulate. The fissioning nuclei are formed in nuclear reactions and the hypothesis of a perfectly equilibrated nucleus undergoing fission is not quite realistic in most of the experiments: the temperature, mass, charge and fission barrier of the initial nucleus are actually defined by the particle emission that takes place during the reaction and equilibration times. Furthermore, after this equilibration, the dynamical evolution of the nucleus is not adiabatic. Therefore, the time scale for particle evaporation, modifying the temperature as well as the fission barrier all along the process, plays an essential role.

2.1. Time to decide to fission

Very few models [10–14] treat simultaneously the dynamical evolution of the nucleus toward scission and the light particle emission due to the conceptual difficulties of such approaches as well as to the unrealistic computer times that they

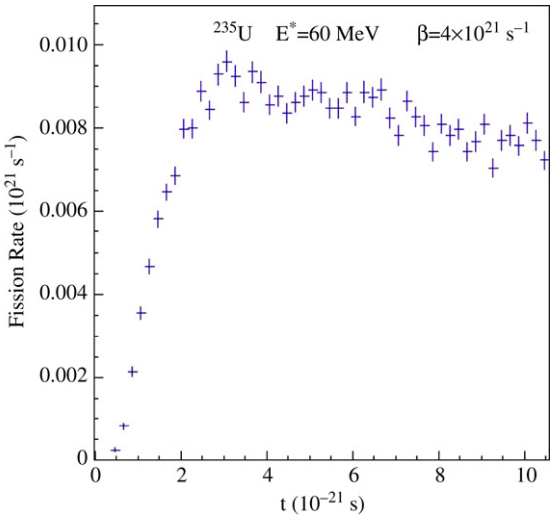

Fig. 1. Fission rate as a function of time calculated with the code CDSM [10] for ^{235}U nuclei excited at 60 MeV with a friction parameter $\beta = 4 \times 10^{21}$ s^{-1}.

would imply in many cases. Therefore most of the data analyses are done with the help of more or less elaborate statistical codes in which the competition between fission and evaporation is calculated according to the Bohr and Wheeler approach, considering a transition state for fission at the saddle point. In the analyses where no dissipation is assumed inside the saddle point, the full Bohr and Wheeler statistical widths Γ^{BW} are used (including sometimes a correction proposed by Strutinsky [15] to take into account the collective states in the available phase space), whereas in the analyses assuming dissipation Γ^{BW} is often reduced to $\Gamma^{K}_{\text{fission}}$ according to Kramers' formulation:

$$\Gamma^{K}_{\text{fission}} = \frac{\hbar\,\omega_{gs}}{T}\left(\sqrt{1+\left(\frac{\beta}{2\,\omega_{sd}}\right)^{2}}-\frac{\beta}{2\,\omega_{sd}}\right)\,\Gamma^{BW} \tag{1}$$

where β is a friction parameter, T the temperature, ω_{gs} and ω_{sd} the frequency of the harmonic oscillators considered by Kramers at the ground state and saddle point, respectively. In the analyses performed with this formulation, the approximation $\hbar\,\omega_{sd} = 1$ MeV is commonly used. In some cases, the correction factor $\hbar\,\omega_{gs}/T$ suggested by Strutinsky [15] is not considered. When considered, the approximation $\hbar\,\omega_{gs} = 1$ MeV is usually done. The validity of these approximations should however be checked, especially for weakly fissile nuclei. Despite the fact that the time is not explicitly present in these approaches, it can be inferred for each of the de-excitation steps from the relation between the total width statistically available Γ_{tot} (due to particle emission as well as to fission) and the lifetime τ of the nucleus: $\tau = \hbar/\Gamma_{tot}$.

2.1.1. Transient time

Examples of calculated time evolutions of the fission rates for ^{235}U and ^{208}Pb nuclei are shown in Figs. 1 and 2. The fission rates have been calculated with the code CDSM [10,11], coupling a statistical emission of light particles and γ-rays with a dynamical description of the fission process through a numerical solution of a one-dimensional Langevin equation. A transient time is clearly seen in both cases corresponding to the rise of the fission rate up to its maximum value. The existence of a transient time before reaching a stationary fission rate had been initially mentioned by Grangé et al. [6] from a solution of a Fokker–Plank equation in which no evaporation was considered. In the present case, due to evaporation during the transient times, quasi-stationary rates are not reached. For uranium, due to its high fissility that makes fission a highly probable channel even at low excitation energies, the fission rate slowly decreases with time after its maximum. By contrast, the lead fission rate is lower than the uranium one, due to the much lower fissility, and it decreases much more rapidly, due to particle emission that removes excitation energy and thus makes the passage over the saddle point more and more difficult.

Considering Figs. 1 and 2 it seems essential to take transient times properly into account due to the important modifications of the nucleus (temperature, fission barrier) that can result, especially for weakly fissile nuclei. Even when no friction effects are considered, a small transient time should exist, corresponding to the dynamical evolution of the nucleus from its equilibrium shape up to the saddle deformation and, especially at high excitation energies, the nucleus can cool down during this period. However, the actual importance, and even the existence, of such a transient time is still under debate. From calculations performed with the mean first passage theory, Hofmann and Ivanyuk [16] claim that there is no room for a transient effect. Within this approach, transient effects affect only a minor part of the initial population, the one that reaches rapidly the barrier, whereas the largest part is still inside the barrier and should not suffer any transient effect. The inclusion of transient effects in statistical models may thus be quite questionable. In addition, Hofmann and

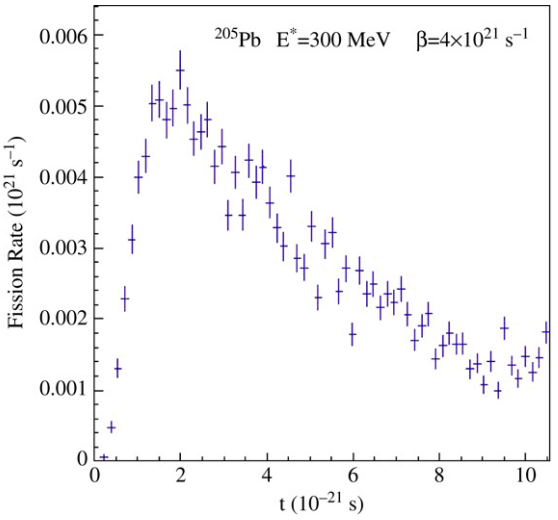

Fig. 2. Fission rate as a function of time calculated with the code CDSM [10] for ^{205}Pb nuclei excited at 300 MeV with a friction parameter $\beta = 4 \times 10^{21}$ s^{-1}.

Ivanyuk [16] underline that in dynamical calculations, the transient time arises from the spreading in deformation space of the particle probability distribution and depends thus on the assumed initial conditions, as already pointed out in [17]. A realistic description should start from a finite width in deformation and momentum, actually corresponding to the initial population after the reaction under study.

An overview of the present experimental results on transient time will be given in Section 4.

2.1.2. Passage over the saddle point (statistical time)

As shown by the time evolution of the fission rates inferred from a numerical solution of a one-dimensional Langevin equation (Figs. 1 and 2), the time needed to pass the saddle point is much longer on average than the transient time: very few nuclei will undergo fission during the transient time and most of the initial nuclei will survive against fission at much longer times. Fission time distributions of ^{235}U nuclei excited at 120 MeV have been calculated in Reference [18] within a statistical approach for different friction coefficients β. The calculations have been performed with level density parameters taken for ground state and saddle point deformations according to the parametrization of Töke and Swiatecki [19]. In the calculations, transient effects were simulated from a reduction of the Kramers' fission widths by a time dependent function determined from fits to numerical solutions of a one-dimensional Langevin equation. The resulting distributions shown in Fig. 3 are very broad, essentially due to the kinetic energy distributions of the particles evaporated before fission is decided (the sometimes used approximation considering only the average kinetic energies of the emitted particles leads indeed to strong underestimations of the times due to the non-linear dependence of the lifetimes on the residual excitation energies). Fig. 3 shows that the time distributions can be fully characterized neither by their most probable or average values, nor by their variances. It shows however that the average values, resulting essentially from tails at very long times ($t \gtrsim 10^{-18}$ s), are quite sensitive to the friction considered, as predicted in [20].

The high sensitivity of the fission yields at very long times has been exploited to determine the evolution with temperature of the friction inside the saddle point, at small deformation (see Section 3). The statistical fission time distribution has also been used in various experiments to distinguish in the super-heavy element region between fusion reactions followed by fission and the supposed much faster quasi-fission reactions. Recent data indicate that the tails at very long fission times might be a quite sensitive probe into the super-heavy element stability, in the region where synthesis becomes unreachable (see Section 3.2).

2.2. Saddle-to-scission time

The saddle-to-scission times are usually inferred through models reproducing observables sensitive to the whole process time, from the initial interaction between the projectile and the target nuclei up to the full acceleration of the fission fragments. Most of the experimental information comes from the pre-scission particle multiplicity, shared between pre-saddle and post-saddle emission (see the review paper by Hilscher and Rossner [8] for a description of the pre-scission measurements). Since both the deformation and the temperature are different inside and outside the saddle point, different dependencies of the friction either on the temperature, or on deformation, or on both, allow a reproduction of the measured total pre-scission multiplicities. Furthermore, due to the large deformations reached at the scission point, the dependence of the level densities, of the binding energies and kinetic energies of the emitted particles play an essential role in the results.

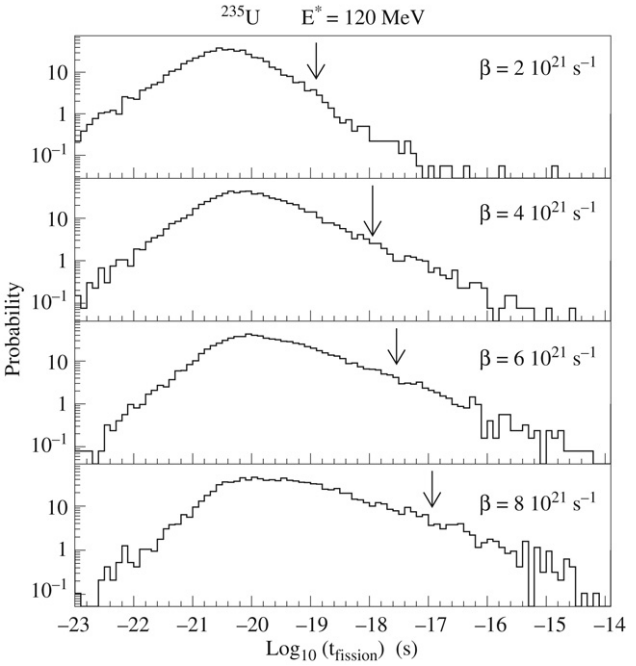

Fig. 3. Fission time distributions (*statistical times)* calculated for different friction coefficients β [18] (the probabilities on the Y axis have not been normalized). The arrows indicate the average time for each distribution.

Lestone et al. [21] have estimated possible effects of the deformation on the charged particle and neutron emission. The left part of Fig. 4 from [21] indicates, for an axially deformed nucleus along a symmetry axis, a large decrease of the average charged particle kinetic energies with deformation, whereas the neutron energies are only weakly modified. This behavior is in agreement with the expected decrease of the Coulomb barrier for charged particle emission when the deformation increases. However, according to Lestone the binding energy B_{part} of a particle strongly depends on deformation:

$$B_{\text{part}} = M_{\text{part}} + M_d^s + D_d(\alpha_i) - M_p^s - D_p(\alpha_i) \tag{2}$$

where M_{part} is the mass of the emitted particle and the α_i are parameters describing the nuclear shape. D_d (D_p) is the deformation energy of the daughter (parent) nucleus that has to be added to its spherical mass M_d^s (M_p^s). Considering masses and deformation energies from the rotating liquid drop model of Reference [22], the resulting change in particle binding energies with respect to the spherical shape is shown for a ^{195}Pb nucleus in the the right part of Fig. 4 that indicates a large increase with deformation of the charged particle binding and a small decrease of the neutron one. For nuclei with A$\sim$ 200, the modification of the binding energies results in a suppression of the charged particle emission larger than the enhancement due to the decrease of the Coulomb barrier. Due to these opposite effects, a large part of the pre-scission emission, at least for neutrons, might take place between the saddle and the scission points (see Section 4), especially if no dissipation is considered inside the saddle.

3. Time for fission decision

As mentioned in Section 2.1.2, the time needed to decide fission has most likely the very same dynamical origin as the transient time, but the long values possibly reached imply statistical treatments of the fission-evaporation competition in most of the data analyses. Therefore this time is often referred to as a *statistical time* in the literature and we shall use this denomination in the following. The discrimination from the *dynamical times* discussed in the next chapter, essentially the transient and the saddle-to-scission times, is therefore somewhat arbitrary. *Dynamical times* are usually appreciably shorter than *statistical times* as illustrated as well by Fig. 3 from [18], with fission statistical widths reduced according to Kramers' formulation by friction effects, as by Fig. 5 from [23] where the full Bohr and Wheeler statistical widths have been considered. For the system considered in Fig. 5 *dynamical times* in the range 10^{-21}–10^{-20}s have been inferred [23] (see Section 4 Fig. 25), whereas, from the very same analysis, a median scission time (the time by which half of the scissions have occurred) longer than 10^{-19} s is obtained. The median scission time is found in Reference [23] to decrease with excitation energy, reaching times of the order of the dynamical times above about 150 MeV. Therefore, as exemplified by Figs. 3 and 5, the *statistical times* are sensitive probes into friction magnitude and evolution with nuclear temperature. Section 3.1 will summarize the most recent experimental results inferred from *statistical times* concerning friction.

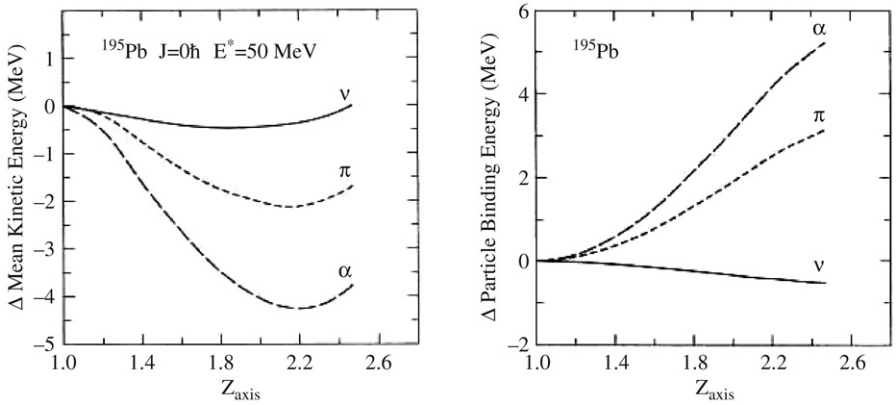

Fig. 4. Change of the mean kinetic energy and binding energy for neutron, proton and alpha particle as a function of the elongation Z_{axis} along the symmetry axis (in units of the diameter of the spherical system). Figure from [21].

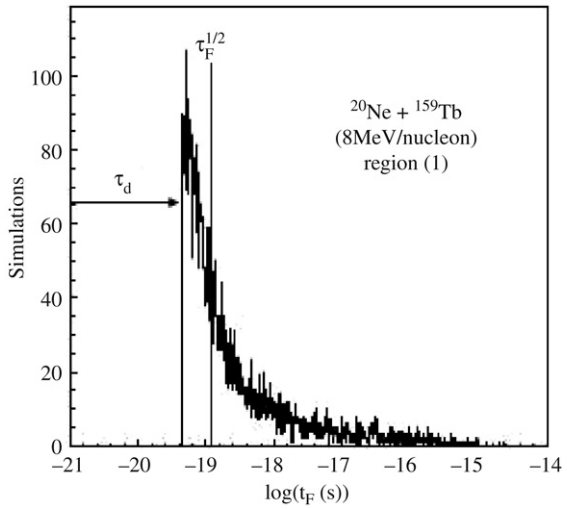

Fig. 5. Scission time distributions as calculated by GEMINI [24] without Kramers width reduction. Figure from [23].

The *statistical time* distributions do not only depend on friction, but obviously depend also on the height of the fission barrier that must be overcome. Therefore, investigations of the average values of the time distributions, of their variances and extensions towards long times give access to information on the nuclear stability of nuclei, directly linked to the fission barrier heights. These possibilities have been explored in recent studies involving reactions between very heavy nuclei that could lead to super-heavy element formation by fusion. Longer *statistical times* are expected for fission following fusion than for the dominant quasi-fission processes in which a compound nucleus is not formed. Fission time measurements, performed on the dominant decay channel, may thus constitute an interesting alternative to direct synthesis experiments to probe the stability of super-heavy elements. Promising fission time studies in the super-heavy mass region will be presented in Section 3.2.

3.1. Nuclear dissipation

Since the first data on pre-scission neutron multiplicities [4,5] and their interpretation in term of nuclear viscosity effects [6,25], important efforts have been made to infer from pre-scission multiplicity experiments fission time scales. Hilscher and Rossner [8] summarize the very first approaches followed in the analyses of pre-scission neutron multiplicity experiments in which the pre-scission emission was assumed to arise dominantly from inside the saddle point and saddle-to-scission emission was not considered. Fission time scales were inferred in such approaches from a reproduction of the pre- and post-scission multiplicities by statistical calculations. However, the assumption of negligible emission yields between the saddle and the scission points can no longer be considered as realistic, at least for neutron emission, due to strong possible effects of deformation and temperature on the binding energies and kinetic energies (see for instance Fig. 4): post-saddle emission contributes in a quite significant way to the pre-scission multiplicities (see Section 4).

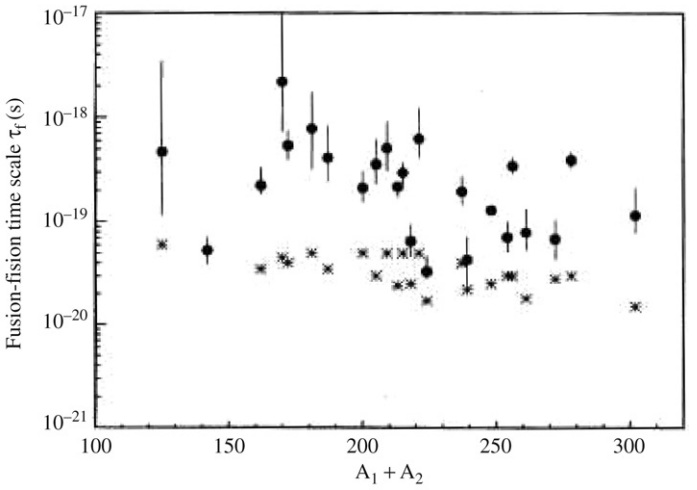

Fig. 6. Comparison of the average fusion–fission times inferred from pre-scission neutron multiplicities with (full points) or without (asterisks) dynamical effects. Figure from [26].

Nowadays, data analyses try to unfold the pre- and post-saddle emission [21,27,23], but the huge uncertainties on the level densities, on the binding energies, on the kinetic energies make the conclusions of such analyses highly model dependent. Time determination from pre-scission GDR γ-rays (see for instance [28–32]) should not in principle be affected by uncertainties on binding energies and removed kinetic energy. They do, however, still depend on the assumed variation of level density with deformation and temperature. Furthermore, as stressed by Siwek-Wilczyńska and collaborators [26], the dynamics of the fusion–fission process can modify in a quite sensitive way the characteristics (mass, charge, temperature) of the nuclei to be considered for the statistical competition between fission and evaporation. Fig. 6 shows for instance as full dots the average fission times inferred from measured neutron multiplicities [33] when they are reproduced using a model coupling the dynamical evolution of the collisions, calculated by the code HICOL [34], with a statistical deexcitation. Within these coupled models, the average *statistical times* are strongly increased with respect to the ones presented as asterisks, inferred by neglecting dynamical effects using the very same data [33].

Despite the large uncertainties on the average *statistical times* from pre-scission emission, it is quite difficult to reconcile the time scales obtained with these nuclear clocks with those measured by two direct techniques, the blocking technique in single crystals [36–38] or the filling of vacancies in the inner electronic shells of the atoms [39,40]: the time scales inferred from the latter are longer by orders of magnitude. Such a discrepancy can be understood considering the poor sensitivity of pre-scission emission to very long times, as shown by Fig. 7 from [35]. It presents, for an excited uranium nuclei without spin (left column) and for excited thorium nuclei with spins resulting from fusion reactions (right column), the scission time distribution, the pre-scission neutron emission time distribution and the pre-scission γ-ray emission time distribution in the upper, middle and lower bin, respectively. They have been calculated with a three step Monte Carlo model, CDSM2 [13, 14], combining statistical and dynamical approaches. In the first step, the dynamical evolution of the nucleus is followed as a function of deformation and asymmetry through a numerical solution of the Langevin equation. For long times, when a quasi-stationary regime is reached, the second step takes place, consisting of statistical calculations of the competition between fission and evaporation. Finally, the last step dynamically follows the evolution up to scission once the fission is decided by either of the two previous steps. The dynamical calculations are performed for very short time steps and the particle emission is calculated at each of these steps. All along the calculations, a one body dissipation reduced by a factor 0.45 is taken into account (0.45 is the value determined in [35] to reproduce average scission time of uranium nuclei excited at 80 MeV). Both for the uranium and thorium nuclei, the scission time distributions are much broader than those of pre-scission neutron emission time and, already for the average scission times indicated by arrows, the pre-scission neutron emission presents probabilities much too weak to be experimentally reached. Therefore, pre-scission neutron emission probes only a part of the scission time distributions and the average *statistical times* inferred are too short. By contrast pre-scission γ-rays cover the whole scission time distribution. However, to discriminate GDR γ-rays emitted by the nucleus before scission from those emitted by fission fragments, a selection on the γ-ray energies has to be applied. Its effect is shown in the lower panels of Fig. 7 for a typical energy selection between 7 and 15 MeV: pre-scission γ-rays emitted at long times have low energies and are removed by the selection. Therefore, the pre-scission γ-rays are not sensitive either to the long scission times. Quite similar qualitative conclusions have also been reached from pure statistical calculations, including Kramers' width reduction with friction parameters $\beta \geqslant 2 \times 10^{21}\ s^{-1}$ [41].

The blocking technique in single crystals is one of the direct techniques used to probe the scission time distribution and leading to time scales much longer than the ones inferred from pre-scission emission. It consists in a precise measurement of the angular distributions of the reaction products in the direction of a major axis (or plane) of a single crystal

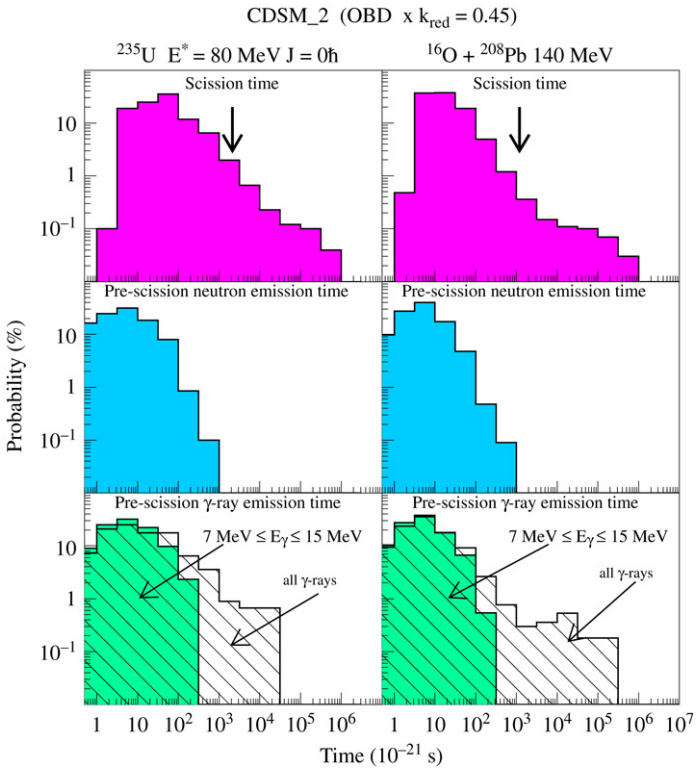

Fig. 7. Distributions of scission times (upper panel), neutrons emitted prior to scission (middle panel) and GDR γ-rays emitted prior to scission (lower panel). Figure from [35].

(for a review of the blocking effects and of the strongly linked channeling effects, see [42]). A fragment emitted precisely in the axis (or plane) direction will be deflected from its initial direction by its atomic interactions with all the atoms of the crystal row (or plane). Dips are thus observed in the angular distribution. The time sensitivity of the blocking effects comes from the dependence of the atomic interactions on the distance from the axis (or plane) at which the detected fragments are emitted by a recoiling nucleus or composite system: the shorter the distance, the stronger the interaction. For a fission process, the blocking effects (the shape of the dip and its depth) are thus directly linked to the scission time. However, they are smeared out by the thermal vibrations of the crystal atoms, leading to a sensitivity limit for the time determination: for a fragment with a given energy and atomic number, the measured dips have the same maximum depth and the same narrowest shape for any emission time shorter than this sensitivity limit. For a fission process the sensitivity limit corresponds to the time needed by the fissioning nucleus to move away from the thermal vibration domain. Therefore, any modification of the blocking patterns with respect to a Reference obtained from short reaction times is a direct evidence for scission times longer than the sensitivity limit. The geometrical origin of the sensitivity limit makes the blocking technique a direct technique, independent of any model, to probe long scission times. Quantitative time information can be obtained by reproducing the measured blocking patterns from simple trajectories simulations taking into account all the atomic interactions in the crystal. Such trajectory simulations imply very few parameters that can be adjusted from blocking patterns measured for reactions with time scales much shorter than the sensitivity limit (for instance elastic or quasi-elastic scattering).

The blocking technique in single crystals has been used in Reference [38] to study the evolution of the scission time distributions and of their average values with the temperature of the initially formed nucleus. In this experiment, excited uranium-like nuclei were formed in deep-inelastic reactions induced by 24 MeV/nucleon uranium projectiles on a silicon single crystal target. The two coincident fission fragments were detected in coincidence and identified in atomic number and energy. The neutron multiplicity was measured in coincidence with the fission fragments with a high efficiency thanks to ORION, a 4π neutron detector filled with gadolinium loaded liquid scintillator. The temperature of the uranium-like nuclei formed in the reaction, before any cooling, could thus be estimated from the strong correlation existing for uranium-like nuclei between the total neutron multiplicity and thermal excitation energy. The blocking effects experienced by one of the fission fragments detected at 7° with respect to the uranium beam direction, in the direction of a ⟨110⟩ axis of the silicon crystal, were measured by silicon position sensitive detectors. At this angle, due to reverse kinematics that lead to high velocities of the fissioning projectile-fragments, a rather short sensitivity limit of 3×10^{-19} s was reached. Blocking patterns for fission of uranium-like nuclei are presented in Fig. 8 for different detected neutron multiplicity bins. As stressed in the previous paragraph, the observed evolution of the dips

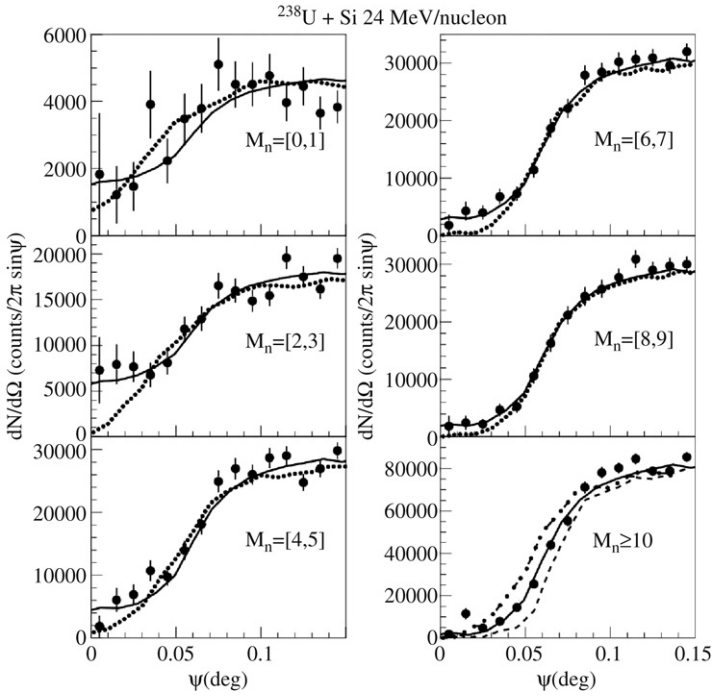

Fig. 8. Blocking dips for fission fragments of uranium-like nuclei. The dips are presented for different bins of measured total neutron multiplicity. The solid curves show examples of fits including different proportions of long lifetime components. The dotted curves show fits obtained for a single lifetime leading to exponential shaped time distributions. See text for the other curves. Figure from [38].

with the neutron multiplicity is a direct evidence for the presence of sizeable components with scission times larger than 3×10^{-19} s, the limit arising from thermal vibrations. A more sensitive way to get evidence for these long time components can be obtained by integrating the yields in the dips. The upper part of Fig. 9 presents the blocking ratio (the yields of Fig. 8, normalized to the yields measured with a random orientation of the crystal and integrated between $\psi = 0.01°$ and $\psi = 0.08°$) as a function of the thermal excitation energy of the uranium-like nuclei. The dashed line indicates the blocking ratio corresponding to scissions occurring at times shorter than the sensitivity limit. It was determined from the blocking pattern measured in the same experiment for elastic scattering detected at 1°, taking into account the differences in charge states and energies for the atomic interactions. Up to excitation energies of about 250 MeV ($T \approx 3$ MeV), the blocking ratio indicates sizable cross-sections of scissions at times longer than 3×10^{-19} s.

The same conclusion has been reached from full simulations of the blocking patterns. For excitation energies above 250 MeV, the blocking dips measured for any neutron multiplicity can be reproduced without any component at times longer than 3×10^{-19} s, provided the effect of post-scission neutron emission is taken into account. The full curve in Fig. 8 shows for multiplicities larger than 10, corresponding to excitation energies above 250 MeV, the result of simulations including post-scission emission, whereas the dashed line shows the result of the same simulations without post-scission emission. The dashed-dotted line shows for comparison the dip simulated assuming an exponential decay law with a lifetime $\tau = 10^{-18}$ s. By contrast, below $T \approx 3$ MeV, the dips can only be reproduced if components at times longer than 3×10^{-19} s are included in the simulations. Two examples of simulations are shown by dashed and full curves for neutron multiplicities lower than 10 in Fig. 8. The dashed curves correspond to simulations in which a single exponential component has been considered in the simulations. In this case, the lifetime, adjusted for each neutron bin, had to be longer than the sensitivity limit to fit the part of the dips at large ψ angles. Nevertheless, it was impossible to reproduce at the same time the central part of the dip, clearly indicating broad scission time distributions in which components with lifetimes longer than the one inferred from the fit with a single exponential have sizable weights. The full curves have been obtained assuming a more complex scission time distribution with a component at times shorter than the sensitivity limit and a component at longer times. An arbitrary shape has been chosen for the latter (a constant probability density between 3×10^{-19} s and 6×10^{-17} s) and its weight has been adjusted for each neutron bin to reproduce the measured dip. With such an arbitrarily chosen distribution satisfactory fits are obtained. Nevertheless, due to rather poor statistics, quite different arbitrarily assumed shapes give similar quality fits, leading to different proportions of events at long scission times and thus to different average values for the distributions. Therefore, the ranges of average values corresponding to the scission time distributions reproducing the measured dips have been determined considering two extreme distributions. The shortest possible average values (lower limits of the bars in Fig. 9) correspond to the fits with a pure exponential distribution. As shown by the dotted curves of Fig. 8, the dips cannot be reproduced with an exponential scission time distribution, but components with

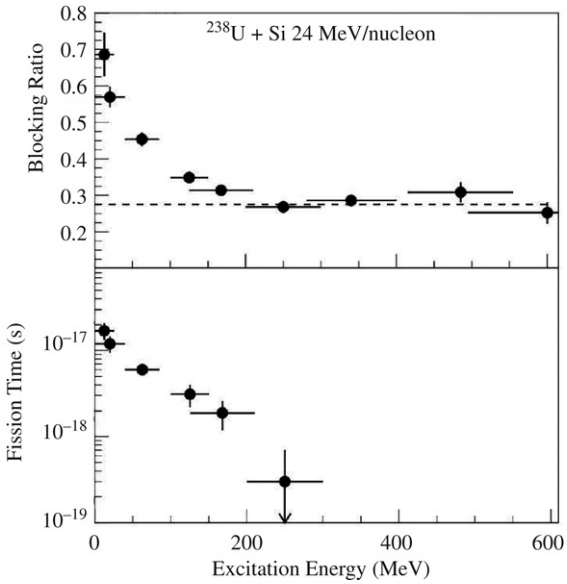

Fig. 9. Upper part: Blocking ratio (a representation of the filling of the blocking dips) as a function of excitation energy. Lower part: Average scission time as a function of the initial excitation energy of the fissioning uranium-like nucleus. The points correspond to average times in bins of excitation energy indicated by the horizontal bars. Figure from [38].

longer lifetimes must be included resulting thus in an overall increase of the average values. The longest possible values (upper limits of the bars) have been inferred assuming a bimodal distribution with components at times below the sensitivity limit and components with very long lifetimes, leading to flat angular contributions to the measured dip (due to the finite spacing between the crystal rows, no dip is observed for components with very long lifetimes). The lifetime associated to these very long time components has been fixed at 10^{-16} s considering the very low residual excitation energies reached at that time, close to the fission barriers, and largely removed by increasing competition with γ-ray emission (if a lifetime longer than 10^{-16} s had been assigned to these components, the upper limits of the bars in Fig. 9 would be still longer). The two distributions considered to determine the time domains presented in Fig. 9 are obviously unrealistic. Realistic time distributions have to consider components with lifetimes between the sensitivity limit and 10^{-16} s. Including such intermediate time components implies weaker weights for the components at 10^{-16} s and therefore shorter average values of the time distributions. The average scission times determined in such a way are presented in the lower part of Fig. 9 as a function of the initial excitation energy. They decrease in an exponential way from a few 10^{-17} s for an initial excitation energy of about 15 MeV down to 3×10^{-19} s for excitation energies of about 250 MeV. For the sake of comparison, the average times from pre-scission neutrons shown in Fig. 6 for masses in the region of uranium are at most of a few 10^{-19} s and correspond to excitation energies below 100 MeV. They are thus at least one order of magnitude shorter than those inferred from the blocking technique.

The time scale for the scission of uranium-like nuclei has also been investigated through a quite different experimental approach based on an atomic clock, the filling of vacancies created in the inner electronic shells during the collisions. During a central atomic collision, electrons are knocked out of the inner atomic shells with a given probability. The vacancies created are then filled in by electrons from outer shells, resulting in X-ray emission with an energy characteristic of the nucleus. If the nucleus formed in the collision undergoes fission, the characteristic X-ray energy permits one to discriminate between emission from the nucleus before scission and from the fission fragments. The lifetimes of K vacancies have been accurately determined from the natural line widths of the rays [43]. Therefore, assuming exponential decay laws for both the atomic and nuclear processes, the probability of detecting a K X-ray characteristic of the nucleus before its scission in coincidence with fission fragments determines in principle the nuclear lifetime, provided the probability of vacancy creation during the collision is known. However, the assumption of an exponential decay law for fission leads, as in the case of the blocking technique, to an underestimation of the average scission times. In addition, corrections have to be applied to take into account the actual populations of electrons in the outer shells that might modify the atomic lifetime. Finally, Wilschut and Kravchuk [40] have shown, from a molecular orbiting theory developed by Anohlt [44], that the widths of the characteristic X-rays might increase during the deformation of the fissioning nucleus up to the scission point when the fission times become much shorter than the atomic lifetime of the K vacancies, leading once more to a possible underestimation of the scission times.

In a first experiment, Molitoris et al. studied the uranium fission in the system ^{238}U + ^{238}U at 7.5 MeV/nucleon [39]. The characteristic K X-rays of uranium were measured for reactions in which the two uranium nuclei undergo fission, or only one of them or none of them. Direct evidence for a large fraction of uranium nuclei surviving against fission at a time at least

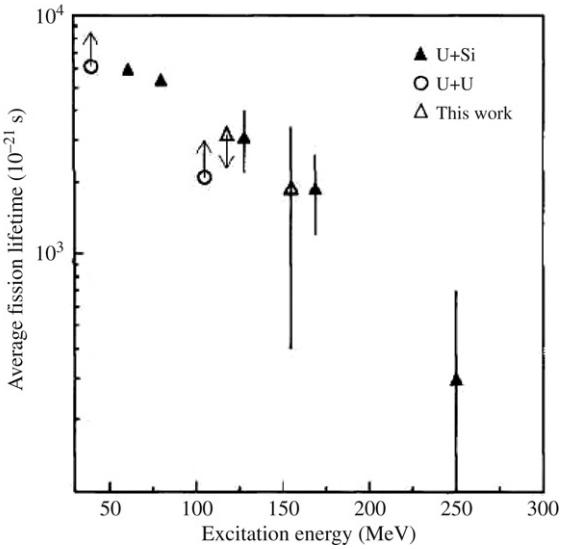

Fig. 10. Comparison of the average scission times from [38] (full triangles, obtained by the blocking technique in single crystal), [39] (open dots, obtained by the K shell vacancy filling method) and [40] (open triangles, obtained by the K shell vacancy filling method). Figure from [40].

of the order of the K vacancy lifetime (7×10^{-18} s) was found from the high measured probability for characteristic X-rays in coincidence with 4 fission fragments: such K X-rays cannot result from vacancies created by internal conversion processes that have lifetimes in the range 10^{-15}–10^{-12} s, much longer than the fission time scales and can only arise from long-lived uranium nuclei. The probabilities of K vacancy creation during the collision have been determined from elastic, quasi-elastic and deep-inelastic reactions in which the two uranium nuclei survived against fission. These probabilities were determined as a function of the reaction Q value in order to take into account vacancy creations during the rather long deep-inelastic reactions preceding fission. Corrections for X-rays arising from internal conversion processes have been determined using the conversion coefficients of detected γ-rays resulting from Coulomb excitation in quasi-elastic reactions. For an initial excitation energy of 40 MeV, a minimum percentage of 77% of fissions were found with scission times longer than 8×10^{-18} s and for 105 MeV, the minimum percentage was 52% for scission times longer than 4×10^{-18} s.

Wilschut and Kravchuk also used the filling of K vacancies to investigate the fission times of excited uranium nuclei [40]. The fissioning nuclei were formed in transfer reactions from ^{20}Ne projectiles at 30 MeV/nucleon to a ^{232}Th target nucleus. The projectile-like fragments escaping from the transfer reactions were detected and identified in charge and mass by 26 phoswich detectors covering a large solid angle in the forward direction starting from 11°. Fission fragments were measured in coincidence by gas detectors and X-rays by Ge detectors. The excitation energy of the target-like fragment after transfer was determined assuming a full energy transfer. The uncertainty due to this assumption on the excitation energies has been estimated from the coincident light charged particle energy and angular distributions. The probabilities for K vacancy creation during the reactions was determined from the characteristic X-ray yield measured in coincidence with elastically scattered neon nuclei. For transfer reactions, a correction was applied to take into account the modification of the atomic number in the entrance channel and in the exit channel. Due to a huge background resulting from Compton effect of γ-rays from the fission fragments, this experiment could only estimate upper limits for the average scission times of uranium nuclei excited at 120 MeV ($\tau_{\text{scission}} < 3.2 \times 10^{-18}$ s) and the average scission time for neptunium nuclei excited at 145 MeV ($\tau_{\text{scission}} = 1.9 \times 10^{-18}$s). The average scission times inferred from non-nuclear clocks (blocking technique and K vacancy filling) have been summarized in Fig. 10 for fission at high excitation energy, leading to symmetric splitting (the percentages associated to minimum time values as given in [39] have been transformed in minimum average scission times). The open dots are from [39], the full triangles from [38] and the open triangles from [40]. It must be stressed that the points reported from [38] include the uncertainties due to the unknown scission time distributions, whereas those from [39,40] have been inferred assuming exponential distributions and thus underestimate the actual values. However, an overall good agreement exists between the three different experiments.

The measured average scission times can be directly compared with calculated *statistical times* since they are longer than the saddle-to-scission times by orders of magnitude. Fig. 11 presents the average *statistical times* calculated by an updated version of the Monte Carlo code SIMDEC [45] either within the pure Bohr and Wheeler approach (without any dissipation) or considering within the Kramers approach a reduced friction parameter β from 2×10^{21} s^{-1} up to 8×10^{21} s^{-1}. The number of cascades has been adjusted in order to get statistical uncertainties on the calculated average fission times within a factor of 2. These statistical uncertainties are most likely responsible for the somewhat irregular behavior of the broken lines joining the calculated points. For the calculations considering friction, in order to take into account a possible transient time at the beginning of the competition between fission and evaporation, a time-dependent statistical fission width has been used,

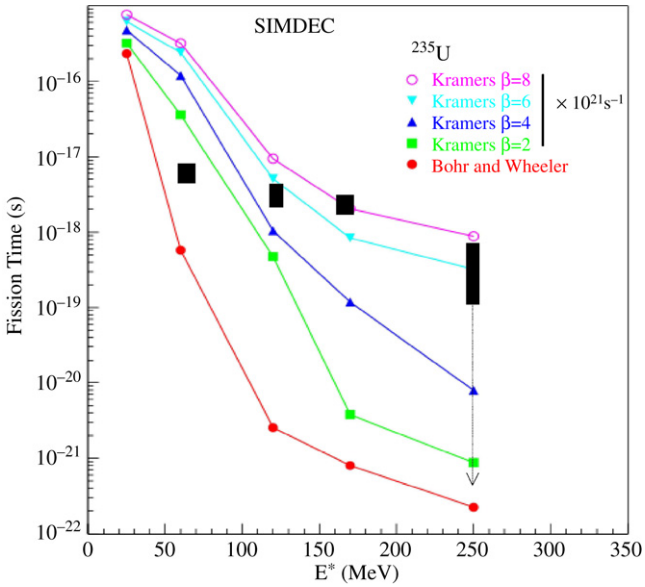

Fig. 11. Average fission times calculated with different friction parameters. The statistical uncertainties on the average values resulting from the Monte Carlo procedure correspond to a factor of 2. The vertical bars are the experimental times from [38]. Adapted from [41].

inferred from numerical solutions of a one dimension Langevin equation. However, the actual evolution of the fission widths during these transient periods does not modify in a sensitive way the behavior of the average fission time curves. Similarly, the inclusion of a transient time when the pure Bohr and Wheeler approach is considered has a very weak influence on the calculated curve. The most sensitive parameters are the deformation dependent level density parameters, taken from Töke and Swiatecki [19] and for the highest energies (above 150 MeV) the light charged particle emission barriers, adjusted on measured particle multiplicities [46,47]. However, attempts to modify these parameters could not affect the following conclusions from the comparison with data. The 4 black rectangles in Fig. 11 indicate the average scission times measured in Reference [38] (the data for excitation energies below 30 MeV have not been included due to the asymmetric behavior of the scissions observed at these energies). For excitation energies above 100 MeV, the pure Bohr and Wheeler approach underestimates by orders of magnitude the average *statistical times* (calculations performed with the same level density parameter at saddle and ground state configurations, lead to calculated average fission times increased by more than one order of magnitude as compared to those obtained with a_f/a_n from [19], but still an agreement for the whole excitation energy range cannot be reached). Up to about 200 MeV, the calculations performed within the Kramers approach reproduce the data only with a friction increasing with excitation energy.

Fig. 12 presents the reduced friction parameters that can be inferred from Fig. 11 as a function of the initial uranium temperature (estimated from $T = (E^* \times 10/A)^{1/2}$). Since each calculated curve in Fig. 11 considers a friction coefficient which does not depend on the excitation energy, the β values presented must be considered as average values along the deexcitation chain of the uranium nuclei, the actual variation with temperature being steeper. Due to the numerous approximations in the calculations (mass and spin of the fissioning uranium nuclei, use of Kramers' formulation …) and to the uncertain level density parameters and charged particle emission barriers, Fig. 12 must only be considered as indicative of the overall tendency for the evolution of β with temperature. Such a qualitative increase of the friction with temperature is indeed expected from various theoretical approaches [48,49].

The evolution of the friction with temperature had already been studied in [29,50,32] for thorium compound nuclei. For ^{224}Th, pre-scission neutron [51] and GDR γ-ray [52,28,53,32] multiplicities, evaporation residue [54,55] and fission [56,57, 55] cross-sections have been determined at various excitation energies up to 118 MeV. Even with a quite strong reduction of the Sierk fission barriers [9] and equal level density parameters for ground state and saddle deformation, it was impossible in [29,32] to reproduce the gamma energy spectra with a standard version of the statistical code Cascade [58] without any friction. Even considering friction, satisfactory agreements between statistical calculations and the data could not be reached when the same constant friction parameter was used for all the excitation energies. In Reference [32], friction $\gamma = \beta/2\omega_{sd}$ (see Eq. (1)) had to be adjusted for each excitation energy in order to reproduce the data with statistical calculations considering the Kramers widths and level density parameters dependent both on deformation, according to [59], and on temperature, according to [60]. The friction parameters obtained are presented as triangles in Fig. 13 as a function of the initial temperature of the ^{224}Th nuclei. A strong increase between 1 and 2.2 MeV is observed. The full line corresponds to a parabolic fit subsequently used in the calculations to adjust the friction at each temperature during the de-excitation process. The results of these statistical calculations are presented as full lines in Fig. 14 together with the data presented as points. The lower left part of the figure corresponds to pre-scission and total neutron multiplicities, the upper left part to γ-ray

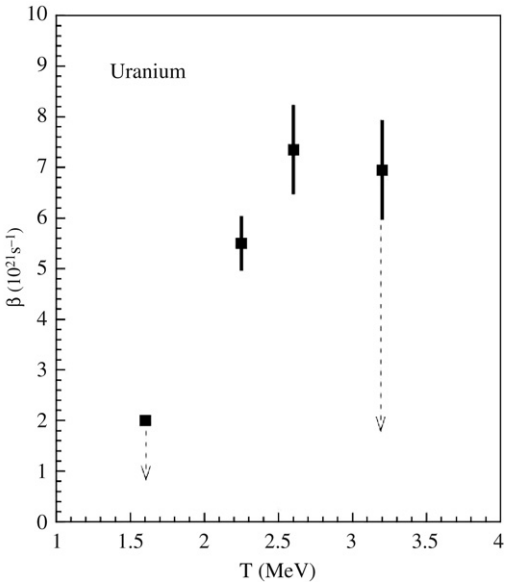

Fig. 12. Reduced friction parameter as a function of the initial temperature of uranium nuclei. Figure from [41].

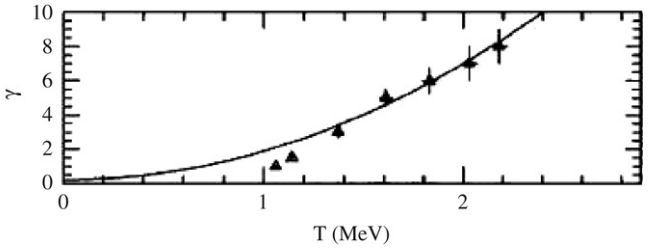

Fig. 13. Friction parameter $\gamma = \beta/2\,\omega_{sd}$ as a function of the initial temperature of ^{224}Th nuclei. Figure from [32].

energy spectra, the upper right part to the spectra of γ-ray excess with respect to the yield calculated for γ-rays from fission fragments (a model dependent way to enhance the representation of pre-scission contributions), and the lower right part to fission and residue cross-sections. All these observables are thus reproduced provided a temperature dependent friction is considered. However, the statistical calculations have been performed assuming an exponential growth of the fission rate during a transient time and in Reference [61] it is mentioned that such an assumption might bias the conclusions. On the other hand, quite satisfactory fits were also obtained in [32] for the same set of data, with the same statistical calculations, by considering a friction coefficient constant with temperature but different inside and outside the saddle point.

In [50], Back et al. were equally unsuccessful in reproducing the evaporation residue excitation function for the $^{32}S + {}^{184}W$ system without friction, whatever the considered level density parameters. From a compilation of existing data, they show, as in the GDR studies for ^{224}Th, an evolution with temperature of the friction parameter. However, two appreciably different evolutions with temperature were found depending on the considered isotope.

The saddle-to-scission times contribute only weakly (see Sections 2.2 and 4) to the long scission times measured by direct techniques that depend thus essentially on the friction inside the saddle point. Therefore, the impossibility to reproduce the measured average times with a constant friction parameter as stressed by Fig. 11 cannot result from a deformation-dependent friction and thus clearly points to a temperature dependency of friction. The friction parameters shown in Fig. 12 are lower than those displayed in Fig. 13 but in the case of GDR γ-rays, the large deformations involved during the saddle-to-scission descent might influence the inferred friction amplitudes if a significant dependency on deformation actually exists. In this case, both the dependencies of friction upon temperature and deformation must be weaker than those inferred considering the two extreme assumptions used in [32].

3.2. Probe into nuclear stability

The fission barriers predicted by liquid drop models vanish for elements with $Z \gtrsim 110$. However, shell effects, expected to be quite large in the vicinity of closed neutron and proton shell structures, might provide for the ground state of some of these super-heavy elements a stability much higher than that of uranium nuclei, for instance. Nevertheless, the various theoretical

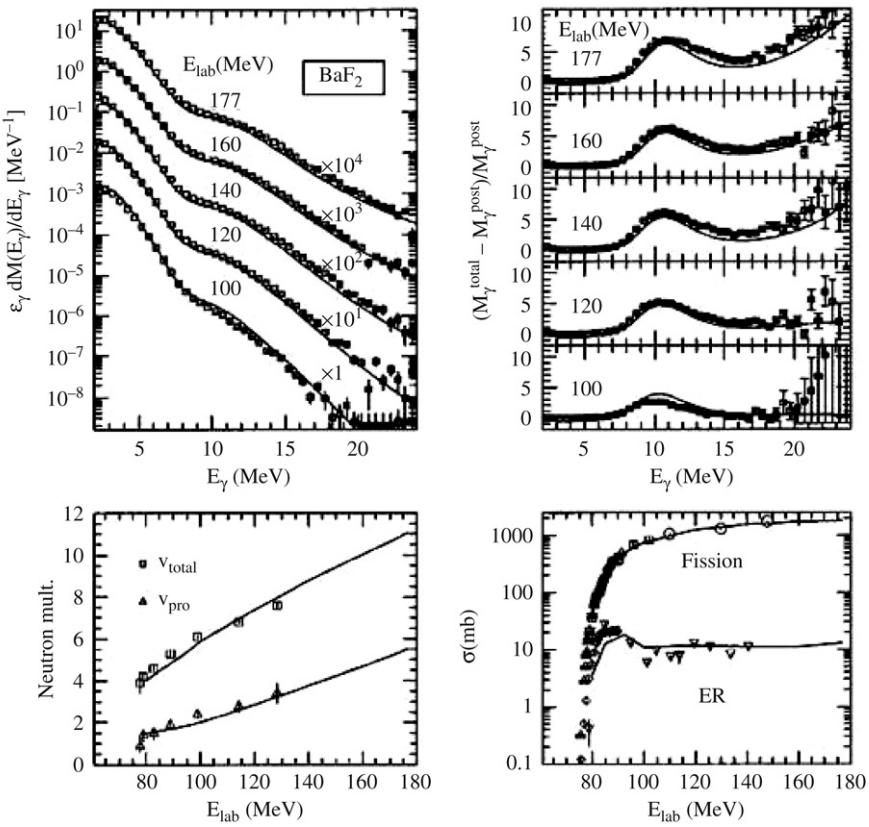

Fig. 14. Experimental observables compared with calculations assuming a temperature dependent friction: γ-ray spectra for different beam energies E_{lab} (upper left part), total and pre-scission neutron multiplicity ν_{tot} and ν_{pre} (lower left), excess of γ-rays with respect to the yield calculated for fission fragments (upper right) and fission and evaporation residue cross-sections (lower right). Figure adapted from [32].

calculations available are neither in agreement on the magic neutron and atomic numbers, nor on the magnitude of the shell effects [62–67]. Therefore, for many years huge experimental efforts have been devoted to the investigation of the stability and structure of super-heavy elements. The most straightforward experimental approach is of course to synthesize these nuclei, but the stabilizing shell effects rapidly vanish with excitation energy, as shown for instance by the fast disappearance of asymmetric fission with temperature, and the synthesis experiments have to face the almost unreachable challenge to form super-heavy elements by fusion reactions between heavy nuclei at low enough excitation energies to give them a (tiny) chance to survive against fission. In addition, in nuclear reactions induced between very heavy ions, the dominant reaction mechanism for central collisions is not fusion, but a fast, out-of-equilibrium, process called quasi-fission. During quasi-fission reactions, the total available kinetic energy can be relaxed and mass is transferred between the projectile and target nuclei, leading for a part of the cross-section to two fission-like fragments with masses and energies similar to those of true fission fragments arising from compound nuclei. The out-of-equilibrium character of the quasi-fission process has been quite directly evidenced from the angular distributions of the emerging fragments, pointing to quasi-fission reaction times smaller than half the rotational period of the composite system [68,69]. For reactions between very heavy nuclei, the quasi-fission cross-section is so dominant that it seems impossible to determine from kinematical analyses if a small proportion of true compound nucleus fission exists among the fission-like fragments. Therefore, a few recent experiments search for evidence of fusion reactions leading to nuclei with $Z \gtrsim 114$, in the region where calculations predict doubly magic nuclei, from the long fission times (at least longer than the quasi-fission reaction times) resulting from the residual shell effects at high excitation energies.

The average pre-scission multiplicities measured for systems in which the fusion–fission process is dominant are found to be appreciably larger than those for systems where quasi-fission is dominant [71,53,72], as expected due to the different time scales involved. Sahu and collaborators have studied [70] the system ^{56}Fe + ^{232}Th at 372 MeV that might lead to compound nuclei with $Z = 116$ by complete fusion reactions. They identified two fission-like fragments in coincidence using two time-of-flight arms. The first one had a parallel-plate avalanche counter used as a start for the two flight times, and the stop was given for each arm by a position sensitive multiwire proportional counter. Neutrons were measured in coincidence by 22 liquid scintillator detectors. For the studied system, quasi-fission reactions are quite dominant, but a hint for a sizable cross-section of fusion followed by fission has been found from the measured mass distributions presented in Fig. 15 for different total kinetic energy bins. The authors interpret these distributions as resulting from the superposition of

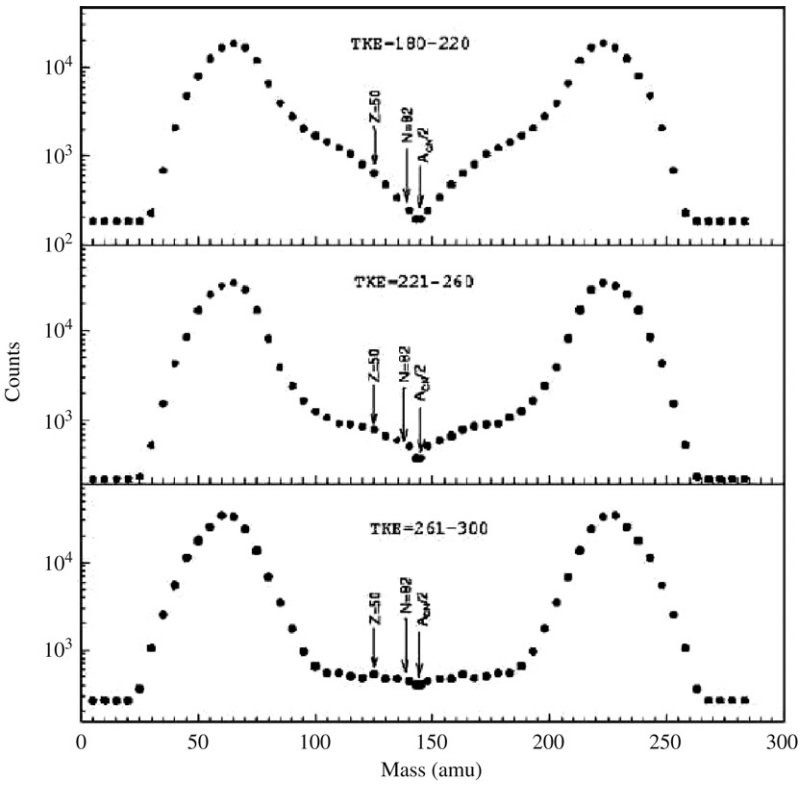

Fig. 15. Mass distributions for different bins of total kinetic energy. Figure from [70].

two distributions, a dominant one corresponding to quasi-fission processes and a second one, leading to the shoulder seen for masses between 120 and 135, corresponding to fusion followed by asymmetric fission (similar interpretations were also given for other systems in the same region [73]). With the assumption that the N/Z ratio of the fragments is the one of the composite system, fragments with the magic proton number $Z = 50$ should have a mass 124 and fragments with the magic neutron number $N = 82$ a mass 137, precisely in the region of the shoulder. The asymmetric mass fission would thus be governed by these magic numbers. The neutron multiplicities in coincidence with fission-like fragments have been used to infer time information. Fig. 16 presents the total (full dots) and pre-scission (open dots) neutron multiplicity as a function of the mass of the light detected fragment. The pre-scission neutron multiplicity increases continuously up to 9 for symmetric splitting where both quasi-fission and compound nucleus fission might contribute. From rough estimates of the neutron binding energies and excitation energies, the time scales for the symmetric splitting deduced from simple statistical calculations are found longer than several 10^{-20} s, much longer than the characteristic time associated with quasi-fission. However, fluctuations might increase the quasi-fission reaction time up to such long values for a part of the cross-section. The behavior of the mass distributions and of the pre-scission multiplicities in this experiment are thus clues for fusion followed by asymmetric fission but more refined analyses are needed.

A very promising analysis of pre-scission particle multiplicity experiments has been made in References [74,75] using backtracing procedures [76]. This analysis technique considers the experimental information as a whole and looks for the correlation between observables providing the best data reproduction. For instance, it permits the determination of the most probable correlation between pre- and post-scission multiplicities from particle spectra measured at fixed given angles in coincidence with fission fragments. In Reference [74], neutron spectra have been measured by the multidetector DEMON [77] in coincidence with fission-like fragments arising from $^{58}\mathrm{Ni} + {}^{208}\mathrm{Pb}$ reactions at 8.86 MeV/nucleon, leading to composite systems with $Z = 110$. The best correlations between various observables were determined from a comparison performed with a backtracing procedure between the data and the results of Monte Carlo simulations considering 3 neutron sources for each fission event: the two fission fragments and the compound nucleus. Fig. 17 presents the correlation obtained between the pre- and post-scission multiplicities for this system. It presents three maxima, at 4, 6 and 8 pre-scission neutrons. The maximum observed at 6 neutrons arises from an odd-even effect resulting from higher neutron binding energies for odd nuclei. The two other maxima have been interpreted as pointing to two different processes, a fast one (quasi-fission) and a slow one (fusion followed by fission) corresponding to 4 and 8 neutrons emitted before scission, respectively. From an improved backtracing procedure, taking into account statistical fluctuations on the measured quantities, a two component pre-scission neutron multiplicity distribution was also inferred in Reference [75] for the system $^{48}\mathrm{Ca} + {}^{244}\mathrm{Pu}$ at 244 MeV in the case of symmetric fission, whereas in the case of very asymmetric fission, only one component was observed.

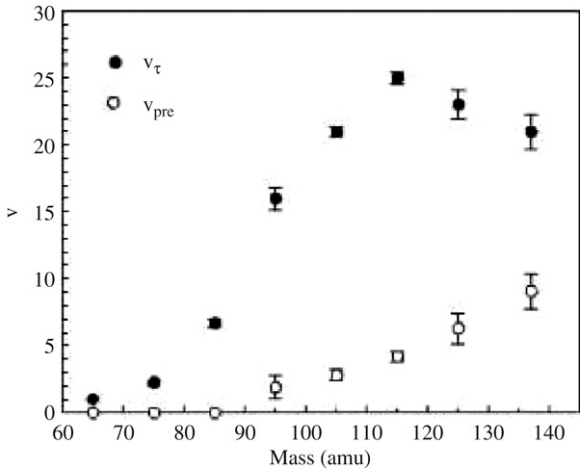

Fig. 16. Total and pre-scission neutron multiplicities as a function of the mass. Figure from [70].

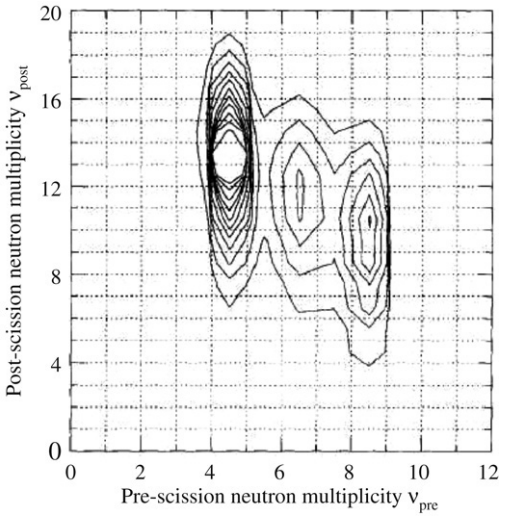

Fig. 17. Correlation between pre- and post-scission neutron multiplicity as inferred from a backtracing procedure. Figure from [74].

The fusion–fission reactions for the system ^{58}Ni + ^{208}Pb at 8.86 MeV/nucleon have been dynamically investigated in [78] with a 3-dimensional Langevin equation, coupled with a statistical model for neutron emission as in the combined dynamical-statistical model described in Reference [11]. For the neutron emission, two different level density parameters have been considered, depending on whether the trajectory is inside or outside a fusion box defined in the deformation space. Temperature and deformation dependent shell effects were included in the potential calculations and a full one-body dissipation was used. The pre-scission neutron multiplicity distribution calculated with these ingredients presents the very same behavior as the one of Fig. 17 inferred from the backtracing analysis with three maxima at 4, 6 and 8 neutrons. The analysis of the trajectories actually shows a quasi-fission component with its maximum at 4 neutrons and a fusion–fission one with its maximum at 8 neutrons, whereas odd-even effects give rise to the maximum at 6 neutrons. Fig. 18 presents the quite different scission time distributions calculated by this model for quasi-fission and fusion–fission trajectories. As expected, the fusion–fission distribution is broader. It extends up to times longer than 10^{-19} s and its maximum is found at a time longer by a factor of about 3 than that of the quasi-fission trajectories. Therefore, both from the experimental analysis using the backtracing procedure and from the model of Reference [78], fusion–fission and quasi-fission processes present significantly different times. However, both approaches are based on a statistical model for the neutron emission and the large resulting uncertainties (due to weak sensitivity of pre-scission emission to long times, dependence of the level densities on deformation, temperature …) must still be considered.

The blocking technique in single crystals has already been described in Section 3.1. A more complete review can be found in [42]. When a nuclear reaction occurs onto a crystalline target atom, the final products feel the potential due to the neighbor lattice atoms. Therefore the ions initially emitted along a crystallographic direction are deflected by the repulsive potential of the atomic strings (or planes) and their angular distribution is thus depleted in this axis or plane direction. The shorter the

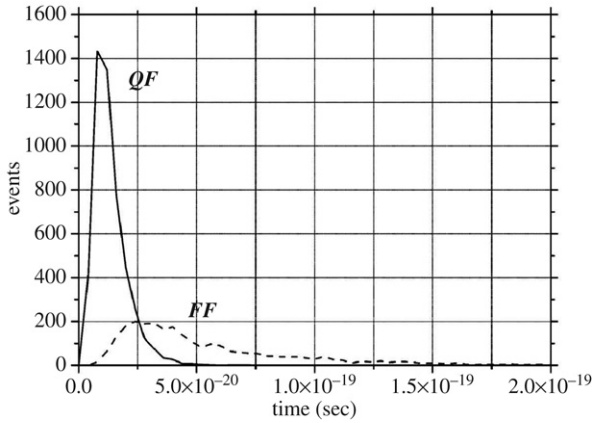

Fig. 18. Scission time distribution for quasi-fission (full line) and for fusion followed by fission (dashed line). Figure from [78].

distance to the atomic row (or plane) for the splitting of the composite system formed during the reaction, the stronger this shadowing effect affects the distribution. For a fission process, the blocking patterns will thus depend on the recoil distance traveled by the fissioning nucleus before scission, therefore on its fission time. The angular distributions plotted as a function of the detection angle ψ of the fragment with respect to the axis direction, presents thus a dip centered at $\psi = 0$. After normalization of the yields with respect to that obtained for an amorphous target, the blocking dips are usually characterized by their yield at $\psi = 0$ (labeled $\chi_{\min}$) and their width $\psi_{1/2}$. The minimum sensitivity limit $t_{\lim}$ of the blocking technique corresponds to the time needed by the composite system to leave the thermal vibration domain of the atoms of the single crystal. Theoretical as well as experimental channeling and blocking studies [42] have demonstrated that for reaction times shorter than $t_{\lim}$, the depths $\chi_{\min}$ of the axial blocking dips are insensitive to the actual reaction time (due to the fluctuating position of the target atoms within the thermal vibration domain) but their widths are proportional to $(Z/E)^{1/2}$ where Z and E are the atomic number and energy of the blocked fragments. The lowest possible $\chi_{\min}$ value is thus reached for any reaction time shorter than $t_{\lim}$ and, for a perfect crystal, it does not depend on the blocked fragment characteristics (mass, charge or energy). However, for a real crystal, the dips can be filled and broadened due to crystal defects and experimental conditions (determination of the axis direction, beam spot size and position, curvature of the targets…). This broadening is all the more significant for the narrowest dips corresponding to the lowest Z/E values. In practice, reaction times longer than $t_{\lim}$ can be evidenced in a selection of events if the associated dip presents a $\chi_{\min}$ value higher than the one obtained for any narrower dip measured for fragments arising from reactions lasting less than $t_{\lim}$. The purely geometrical origin of the sensitivity limit $t_{\lim}$ makes the blocking technique a model independent way to get evidence for long fission times.

The blocking effects associated to fission-like fragments detected at 20° have been measured [18,79–81] for the ^{238}U+Ge system at 6.16 MeV/nucleon, ^{238}U + Ni system at 6.62 MeV/nucleon and the ^{208}Pb + Ge system at 6.16 MeV/nucleon. The compound nuclei possibly formed in these reactions have $Z = 124$, 120 and 114, respectively, and would have rather high excitation energies, up to about 80 MeV. For each of these systems, a sensitivity limit $t_{\lim} \approx 10^{-18}$ s can be easily determined from the center-of-mass velocity, the extension of the thermal vibration domain and the detection angle. The reaction mechanisms involved in these systems have been analysed with the help of INDRA [82], a 4π charged product detection array, providing an identification of all the fragments (Z and E) and light charged particles (Z, A and E). The blocking effects were measured by a telescope located at 20° consisting of a low pressure ionization chamber followed by a two-dimensional position sensitive resistive silicon detector. Fig. 19 presents the measured correlation between the energy loss ΔE in the ionization chamber and the residual energy E_{res} in the silicon detector for the ^{238}U + Ge system at 6.09 MeV/nucleon. Four regions, labeled from *a* to *d*, corresponding to different reaction mechanisms are delimited by contours. The region *a* corresponds to projectile-fragments arising from deep-inelastic collisions. The blocking dips associated to these events provide the $\chi_{\min}$ reference for times obviously shorter than 10^{-18} s. Similarly, the events in region *d* are target-like fragments from quasi- and deep-inelastic reactions and the associated blocking dip also provide the short time Reference. The region *b* is populated by fission-like fragments for which the coincidences with INDRA show that: (i) the kinetic energies as well as the correlation angles are in good agreement with the ones expected for fission following fusion, (ii) the multiplicities of fragments with $Z \geqslant 3$ in coincidence with the two fission-like fragments is negligible and (iii) the coincident light charged particle multiplicity ($Z \leqslant 2$) is of the order of 0.08. The INDRA coincidences thus indicate that the fission-like fragments detected in region *b* arise either from quasi-fission processes in which the available kinetic energy has been fully damped, or from fission following the formation of compound nuclei with $Z = 124$ (it has been checked that removing from the analysis the scarce events with a light charged particle does not affect the conclusions). These fission-like fragments arise from asymmetric scissions, the atomic number corresponding to the maximum yield in zone *b* being $Z \sim 80$. The complementary light fission-like fragment is found in region *c* that is however dominantly populated by fragments from sequential fission of uranium-like fragments excited in quasi- and deep-inelastic reactions. Due to the long scission times of uranium-like nuclei

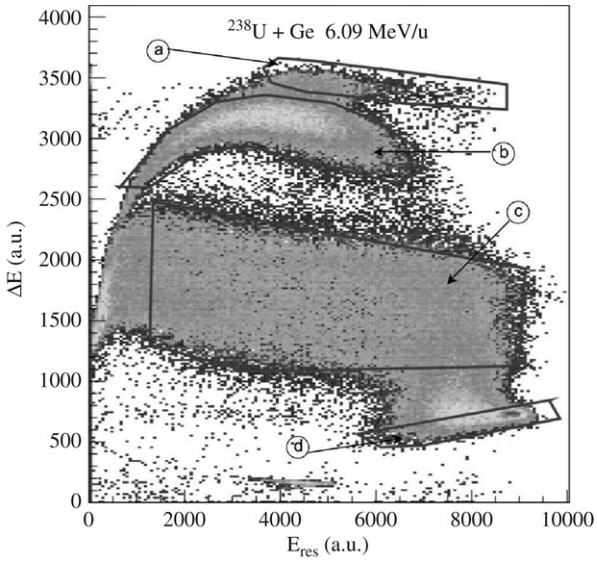

Fig. 19. Energy loss versus residual energy for fragments detected at 20°. Figure from [18].

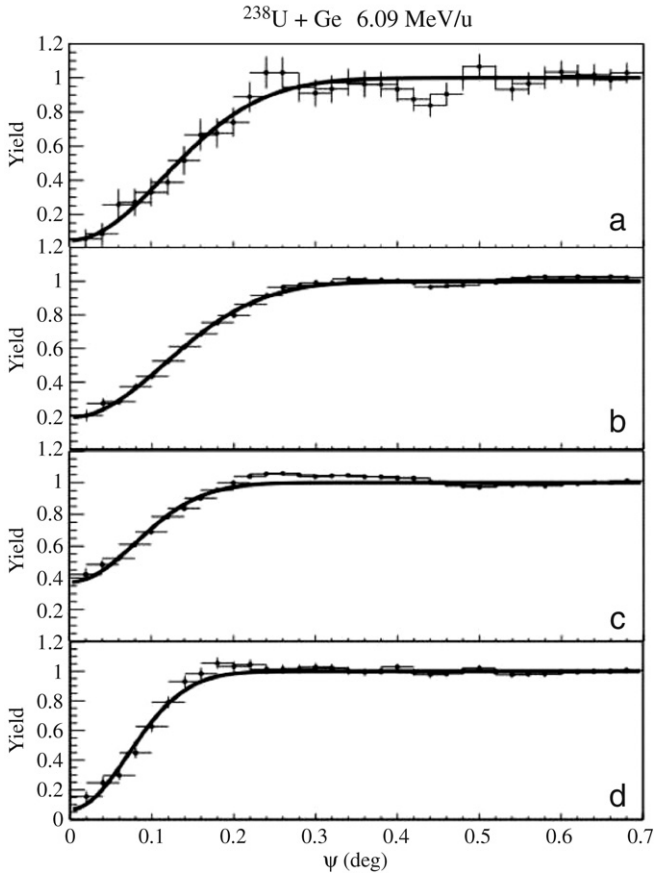

Fig. 20. Blocking dips associated to the 4 regions labeled *a* to *d* in Fig. 19. Figure from [18].

(see Section 3.1), the dip associated to the events in zone *c* can be considered as a test for the blocking technique sensitivity towards long times.

The blocking dips associated to the 4 regions defined in the E_{res}–ΔE plane are shown in Fig. 20 in which the solid lines are Gaussian fit results. The labels *a* to *d* of the 4 panels refer to the event selections indicated in Fig. 19. As expected, the

reactions lasting less than t_{lim} (labels *a* and *d*) lead to dips with similar χ_{min} values, providing a short time reference χ_{min} of the order of 0.08. The very similar χ_{min} measured for the quite different fragment energies and atomic numbers involved in zone *a* and *d* clearly show that no spurious effect from crystal defects or from experimental resolution affects the χ_{min} values. For the sequential fission of uranium-like nuclei (region *c*), a quite large χ_{min} increase with respect to the short time reference results from the long scission times involved [38]. The dip associated with region *b* also presents a significant χ_{min} increase that can only result from reaction times longer than t_{lim}. Since the quasi-fission reaction times have been directly determined for similar systems from the measured angular distributions in ranges between 10^{-21} and 10^{-20} s [68, 69], fission-like fragments arising from composite systems living more than 10^{-18} s can only arise from fission of $Z = 124$ compound nuclei. A minimum proportion of compound nucleus fission events among the fission-like events of region *b* can be estimated with the very rough assumption of two main components in the scission time distribution: a component at times shorter than t_{lim} and another one at very long times giving a flat contribution to the dip. With this rough assumption, a χ_{min} increase from 0.08 (the short time reference) up to $\approx$0.20 (as measured for region *b*) imply proportions of 12% for the long time component and 88% for the short time one. However, realistic time distributions must have contributions from reaction times intermediate between the two extremes considered for this rough estimation. Such intermediate times increase the χ_{min} less efficiently than components giving a flat contribution to the dip. Therefore, the blocking technique provides us with a direct evidence for at least 12% of fission fragments from $Z = 124$ compound nuclei among the fission-like fragments detected at 20°. The compound nuclei formed in this way, as well as all the daughter nuclei after neutron emission, must have sizable fission barriers to survive such long times against fission.

For the ^{238}U + Ni system at 6.62 MeV/nucleon, an evidence for formation of compound nuclei with $Z = 120$ has been also found from the χ_{min} values associated with fission-like events and a similar (within the experimental errors) proportion of $\approx$10% of fusion–fission reactions can be inferred. By contrast, for $Z = 114$, no clear evidence for compound nucleus formation could be found within experimental accuracy. It seems to arise from neutron deficiency with respect to the predicted neutron magic number ($N = 184$ for most of the models) of the compound nuclei and their daughters possibly formed in these reactions: these nuclei have low fission barriers and, if formed, undergo fission very rapidly. Conversely, the high probability for long fission times for $Z = 120$ and 124 indicate high fission barriers, even at the highest excitation energies involved, and thus very strong shell effects most likely progressively restored during de-excitation. Indeed, islands of stability are predicted in this region. Therefore, a systematic investigation of the scission time distributions around these nuclei will provide a confirmation of the existence of stability island(s) in this region.

The investigation of scission times either from pre-scission particles or from blocking effects provide thus pieces of information on the stability of super-heavy elements that could not be reached through other observables. It gives access to a clear discrimination between quasi-fission and fusion–fission events. However, the very long scission times associated to the tails of the distributions probed by the blocking technique seem hardly compatible with the predictions of statistical models when all the parameters have been adjusted to reproduce the tiny heavy residue cross-sections as inferred from synthesis experiments. Such a discrepancy might arise from the extrapolations performed for various parameters towards the super-heavy region as well as from the evolution with temperature and deformation of the level densities and of structure effects (shell and pairing effects).

4. Transient and saddle-to-scission times (dynamical times)

The concept of transient time as it was introduced in the pioneering work of Grangé et al. [6] in the framework of a diffusion model assumes that the internal equilibration time of the heat bath is short compared to the characteristic time of the diffusion process itself and the decay times. The transient time is a key parameter to describe the competitive decay of a compound nucleus as it determines the importance of the particle emission in the early stage of the time evolution. It was introduced to account for unexpectedly large pre-scission neutron multiplicities measured in [4]. Despite its intrinsic dynamical nature, a transient time is now currently mocked-up in statistical calculations by introducing a time-dependent fission width of the form

$$\Gamma_f(t) = f(t) \times \Gamma_f^0 \tag{3}$$

where Γ_f^0 is the fission width as calculated without transient time. The quasi-stationary fission width Γ_f^0 is taken either as the standard Bohr and Wheeler fission width when dissipation is not considered or as the friction-dependent Kramers width of Eq. (1). Different functions $f(t)$ are used: either a simple step function with $f(t) = 0$ for $t < \tau_{trans}$ and $f(t) = 1$ for $t > \tau_{trans}$, or an exponential-type function of the form $f(t) = (1 - \exp -(t/\tau_{trans}))$ or a more complex function inferred in [61] from an analytical solution of the Fokker–Plank equation in the over-damped case, assuming a parabolic nuclear potential. A comparison of the fission rates derived with this analytical function and from a numerical solution of the Fokker–Plank equation is shown in Fig. 21 for different assumed values of the friction parameter β. As expected from the assumptions made to infer the analytical curves, a satisfactory agreement is found only in the over-damped case ($\beta \gtrsim 2 \times 10^{21}$ s^{-1}). The authors of Reference [61] stress the large discrepancy obtained between the friction parameter inferred considering an exponential-type function and those inferred either with a step function or with their analytical formulation which are rather similar.

Depending on the analysis, τ_{trans} is considered as a free parameter adjusted in order to reproduce data, or as a parameter linked to the friction coefficient determining the fission rates at longer times. In the latter case, τ_{trans} is determined from the

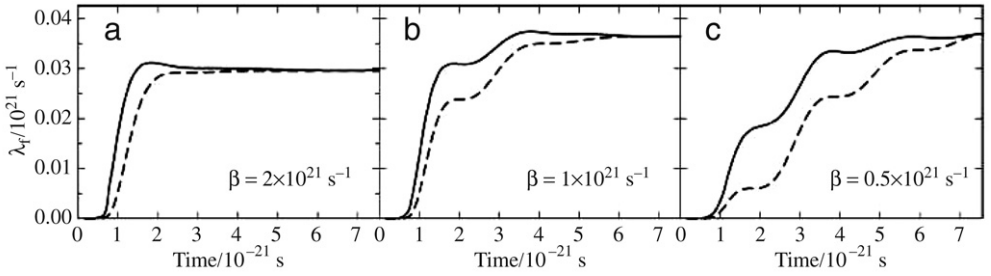

Fig. 21. Comparison of fission rates from a numerical solution of the Fokker–Plank equation (solid curve) and from the analytical approximation of [61] (dashed curve). Figure from [61].

friction either with the formulation of [61] for over-damped cases or with analytical formulations inferred from approximate solutions of a time-dependent Fokker–Plank equation [83,84]:

$$\tau_{\text{trans}} = \frac{\beta}{2\omega_{gs}^2} \ln(10B_f/T) \tag{4}$$

for over-damped cases $\beta > 2\omega_{gs}$ and

$$\tau_{\text{trans}} = \beta^{-1} \ln(10\, B_f/T) \tag{5}$$

for under-damped cases, where B_f is the fission barrier and T the temperature. However, any statistical calculation requires as inputs initial as well as saddle conditions. The dynamics of the different reactions used to form fissioning nuclei are so complex and can play such an important role (see for instance Fig. 6) that the determination of these conditions represents a real challenge that recent experiments have tried to take up.

Nowadays the pre-scission multiplicity measurements are mainly used to extract the fraction of particles emitted inside the saddle point and the ones emitted during the descent from saddle to scission. From these unfolding procedures, transient times, *statistical times* (or sometimes only the sum of transient and *statistical times*) and saddle-to-scission times are deduced. Complementary pieces of information can be extracted from fission probabilities that only depend on transient and *statistical times*, irrespective of the further evolution of the system from saddle to scission. A quite large set of data on pre-scission multiplicities and fission probabilities is available. It covers different production mechanisms for the fissioning nuclei leading to various angular momenta, temperature, deformation …. However, a quite confusing situation exists in the conclusions due to the different analyses undertaken (with or without dissipation, level density parameter dependency upon temperature and deformation …). The dissipation is usually assumed to be the same during the transient and *statistical times* due to similar expected average deformations and temperatures and is considered as a free parameter of the model. If no dissipation is considered, a transient time is nevertheless simulated in the statistical calculations that can be seen as a simple delay to fission arising from the time needed for the deformation of the nucleus up to the saddle configuration and the fission decay widths are calculated within the standard Bohr and Wheeler statistical formalism. An original approach proposed by Moretto [85] scaling fission excitation functions will also be described later in this subsection in which recent and significant results obtained within these different approaches will be presented.

An interesting set of results has been obtained by Ramachandran et al. in [27] from simultaneous measurements of neutron and light charged particle multiplicities. For the 159 MeV ^{28}Si+^{175}Lu system, pre-scission multiplicities of neutrons, protons and alpha particles have been extracted through multi-source fits assuming compound plus (fully accelerated) fission fragment emissions for neutrons and light charged particles with an additional near-scission component for α-particles. However, neither pre-equilibrium emission has been considered, nor any dynamical fusion effect. Calculations have been performed to reproduce all these multiplicities, using the statistical code JOANNE [86] which includes the effect of deformation on particle binding energies and transmission coefficients. The full Bohr and Wheeler widths have been used, but fission could compete with particle evaporation only after a delay time τ_{trans}. The evaporation of particle during the descent time from saddle to scission τ_{ssc} was modeled by considering emission from a system with a deformation somewhere between the saddle and the scission points. Deformation-dependent level densities following the Töke and Swiatecki prescription [19] have been used in the statistical calculations but were simply taken as $A/11$ for the compound nucleus and $A/7$ for the fission fragments in order to extract the temperature in the multi-source analysis. Pre-scission emission has been assumed to take place from two points of the deformation space, corresponding to mean pre-saddle deformation and mean saddle-to-scission deformation, the latter being left as a free parameter as well as the transient (or pre-saddle) time and the post-saddle time. The limits of variation of post-saddle deformation have been fixed between 1.90 and 2.45 considering the potential energy diagram shown in Fig. 22. This analysis is similar to the one presented in [21,86] which detailed the effect of deformation on particle binding energies and transmission coefficients (see Fig. 4): increasing deformation results in a decrease of effective proton and α-particle emission barriers favoring charged particle emission over neutron emission. On the other hand, with increasing deformation, the neutron binding energy decreases slightly whereas charged particle binding energy strongly increases. The balance between these opposite trends allows the authors of [27] to

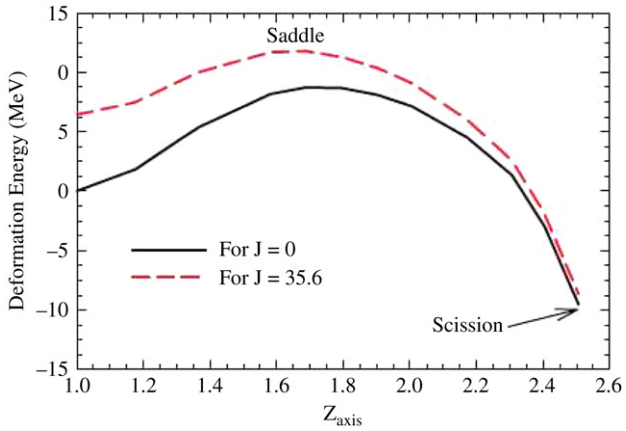

Fig. 22. Potential energy diagram for ^{203}At showing deformation energy as a function of the elongation Z_{axis} along the symmetry axis (in units of the diameter of the spherical system) for angular momentum $J = 0$ and 35.6 $\hbar$ (35.6 $\hbar$ is the average of compound nucleus angular momentum distribution). Figure from [27].

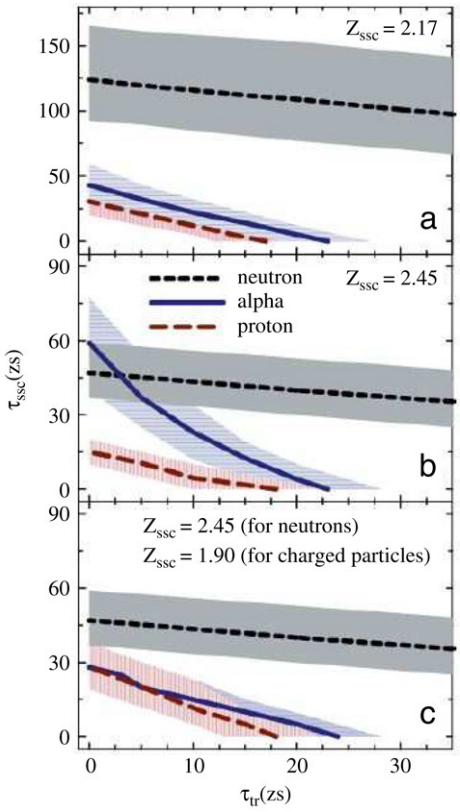

Fig. 23. Combinations of transient times τ_{trans} (noted τ_{tr} on the x-axis) and saddle-to-scission times τ_{ssc} required to reproduce experimental neutron, proton and α pre-scission multiplicities shown as medium dashed, long dashed and solid lines, respectively. Different average post-saddle deformations Z_{ssc} are considered: (a) $Z_{ssc} = 2.17$, (b) $Z_{ssc} = 2.45$, and (c) $Z_{ssc} = 2.45$ for neutron emission and $Z_{ssc} = 1.90$ for charged-particle emission. The shaded regions correspond to experimental errors. Figure from [27].

conclude that on the average neutrons and charged particles are emitted at different steps along the fission path, shown in Fig. 22, and thus are associated with different deformations.

Calculated multiplicities, as a function of τ_{trans} and τ_{ssc} are compared with experimental values in Fig. 23. Considering the dependence of the binding energies on deformation from Reference [21] presented in Section 2.2, the authors could only find an overall agreement assuming that neutron emission occurs closer to scission and charged particle emission closer to saddle. With these assumptions, a very short pre-saddle transient time, less than 2×10^{-21} s and a post-saddle time close

to 4×10^{-20} s can be inferred from the overlapping regions in Fig. 23-c. However, the actual dependence of the binding energies on deformation is still under debate, contributing thus to the large uncertainties on the times inferred from pre-scission neutron and charged particle emission.

In [23] Cabrera and coworkers gathered a quite complete set of data on the systems ^{20}Ne + ^{159}Tb and ^{20}Ne + ^{169}Tm between 8 and 16 MeV/nucleon: fusion-evaporation and fusion–fission cross sections have been measured as well as neutron, proton and α-particle energy spectra at different angles. Neutrons emitted in coincidence with fission fragments were efficiently detected in 96 DEMON counters and light charged particles in 6 telescopes, each consisting of 3 silicon detectors located between 115° and 165°.

Pre- and post-scission multiplicities were extracted by multi-source fits including pre-equilibrium emissions for neutrons, but not for charged particles which were not detected at sufficiently forward angles in these experiments to see this component in the spectra. Only 3 sources (CN + 2 FF) were considered for light charged particles and the non-consideration of near scission emission for α particles results in a poorer quality of the fits around 10 MeV. To reduce the number of free parameters only symmetric fission has been considered. Due to the limited angular coverage of the charged particle detectors, pre-equilibrium particles could not be measured. In order to get the spin and initial excitation energy distributions of the CN required by a statistical model analysis of the data, their multiplicity has been interpolated from existing data. The excitation energy and angular momentum of the compound after pre-equilibrium have then been estimated from the total mass loss through pre-equilibrium emission and linear momentum transfer according to [87]. Statistical model calculations based on the code GEMINI [24] were performed, considering two regions in the angular momentum distribution, corresponding to fusion–fission and fast fission processes. For fission following fusion, standard Bohr and Wheeler transition state formalism was used, with angular momentum dependant fission barriers and spherical transmission coefficients for particle decay widths. A dynamical delay time τ_d^1 during which fission is canceled has been introduced. For the lowest bombarding energy of 8 MeV/nucleon, where fast fission is not observed, τ_d^1 and the level-density parameters a_n and a_f for the ground state and saddle-point configurations, respectively, were adjusted to reproduce the pre- and post- scission multiplicities of n, p, and α-particle and the ratio σ_{Er}/σ_f of the cross-sections for evaporation residue and fission. The level density parameters were then assumed independent of excitation energy and kept constant for the higher bombarding energies. The values of τ_d^1 were then adjusted for each bombarding energy to fit the experimental cross-section ratios σ_{ER}/σ_F. Since for the highest excitation energy, fast fission represents a sizable part of the cross-sections, an other dynamical time τ_d^2 has been introduced. For fast fission, particle emission from the composite was considered during τ_d^2 and assumed to arise from a deformed nucleus with a deformation corresponding to the average one calculated by the dynamical code HICOL [34]. τ_d^2 was then extracted at each bombarding energy from fits of the multiplicities of all the light particles with a weighted average multiplicity ν_i arising both from fusion–fission and fast fission processes:

$$\nu_i = \frac{\nu_i^1(\tau_d^1)\sigma^1 + \nu_i^2(\tau_d^2)\sigma^2}{\sigma^1 + \sigma^2}$$

where σ^1 and σ^2 are the cross sections for each of these two processes and $\nu_i^1(\tau_d^1)$ and $\nu_i^2(\tau_d^2)$ the associated multiplicities. Comparison between experimental and simulated particle multiplicities are presented in Fig. 24 for the ^{20}Ne+^{159}Tb reaction. In Fig. 25 is shown the evolution of the extracted dynamical times τ_d^1 and τ_d^2 with the bombarding energy for the ^{20}Ne+^{159}Tb reaction, which in all cases are of the order of a few 10^{-20}s. It must however be stressed that within this analysis, no emission from saddle to scission is considered. The authors consider that the inferred τ_d^1 can be interpreted as also including the saddle-to-scission time. Such a global unique dynamical time τ_d^1 applied at the beginning of the fission process to account for all the pre-scission multiplicities (pre- and post-saddle) might only be realistic if the post-saddle emission is negligible or if the pre- and post-saddle deformations and temperature were similar. The latter statement seems however in contradiction with the calculated *statistical time* distribution shown in Fig. 5 that implies a strong cooling before the saddle-to-scission descent. The similarity of the two dynamical times and the larger values of τ_d^1 for the lower two bombarding energies lead the authors to suggest that the evolution from a compact composite system to a dinuclear shape may be quite similar for conventional and fast fission, and that the time scale for shape equilibration to be considered in the fusion case, would decrease with energy, maybe indicating a temperature dependence of dissipation.

Experiments measuring fission probabilities present the huge advantage with respect to the ones measuring particle multiplicities to give access to the saddle time rather than to the scission times. An original approach is used by Moretto in [85] to probe the necessity to go beyond the standard transition state description, by examining a large set of fission excitation functions, looking for any deviation from scaling laws derived from the transition state formalism in which the fission cross section σ_f can be written as:

$$\sigma_f = \sigma_0 \frac{\Gamma_f}{\Gamma_T} \approx \sigma_0 \frac{1}{\Gamma_T} \frac{T_s \rho_s(E - B_f - E_r^s)}{2\pi \rho_n(E - E_r^{gs})}. \tag{6}$$

where σ_0 is the fusion cross section, ρ_s and ρ_n are the saddle and ground state level densities, E the excitation energy of the compound nucleus, B_f the fission barrier, T_s the temperature at the saddle and E_r^s et E_r^{gs} the saddle and ground state rotational energies. Assuming the simple expression $\rho(E) \propto \exp(2\sqrt{aE})$ at the saddle point with an effective barrier B_f^*

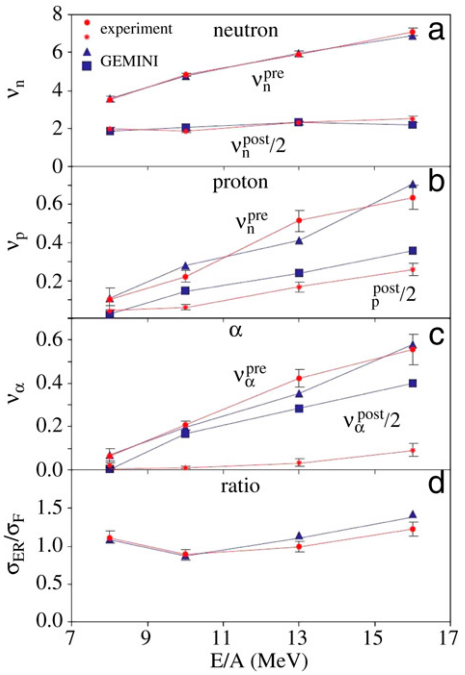

Fig. 24. For the ^{20}Ne + ^{159}Tb reaction, a comparison, as a function of bombarding energy per nucleon E/A, of the experimental pre-scission and post-scission multiplicities with the values calculated by GEMINI for (a) neutrons, (b) protons, and (c) α-particles. The comparison in (d) is for the cross-section ratios σ_{ER}/σ_F. The broken curves are to guide the eye. Figure from [23].

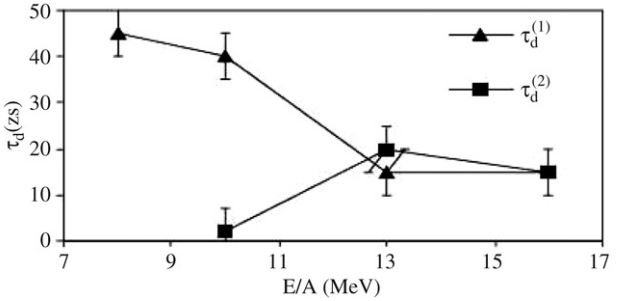

Fig. 25. Evolution with bombarding energy of the dynamical times τ_d^1 and τ_d^2 (see text) extracted from statistical model simulations for the ^{20}Ne + ^{159}Tb reaction. Figure from [23].

which is uncorrected for pairing effects due to significant excitation energy at the top of the barrier, Eq. (6) can be rewritten as:

$$\frac{1}{2\sqrt{a_n}}\ln\left[\frac{\sigma_f}{\sigma_0}\Gamma_T\frac{2\pi\rho_n(E-E_r^{gs})}{T_s}\right]=\frac{\ln R_f}{2\sqrt{a_n}}=\sqrt{\frac{a_f}{a_n}(E-B_f^*-E_r^s)}. \tag{7}$$

Considering the mass region and excitation energy range, the total width Γ_T has been approximated by Γ_n. As the mass range for the fissioning nuclei considered in [85] is quite large ($185 < A < 214$), which may imply strong variation of the shell effects amplitude, consideration of the shell and pairing effects have been taken into account. The lowest excitation energy for the residual nucleus after neutron emission being typically 15–20MeV, the asymptotic exponential expression of the level density ρ_n is assumed to be valid as long as the ground state shell effect Δ_{shell} of the daughter nucleus after neutron emission is considered [88]: $\rho_n(E-B_n-E_r^{gs}) \propto exp(2\sqrt{a_n(E-B_n-E_r^{gs}-\Delta_{\rm shell})})$.

In a first step a fitting procedure of 14 experimental fission excitation functions in the lead region as been performed using Eq. (6), considering as free parameters the shell effects corrections, the effective barriers and the ratio a_f/a_n assuming $a_n = A/8$. The shell correction amplitudes extracted from the fits are in very good agreement with the values determined from the ground state masses. Then with the experimental fission cross-sections and the extracted values of effective barriers and shell corrections, the excitation functions for the 14 compound nuclei scale on a single straight line when, following Eq. (7) the quantity $\ln R_f 2\sqrt{a_n}$ is plotted as a function of the square root of the excitation energy over the saddle. Fig. 26 shows this linear correlation for the ^{201}Tl nucleus. The slope of this line is close to unity indicating a ratio a_f/a_n close to 1. It

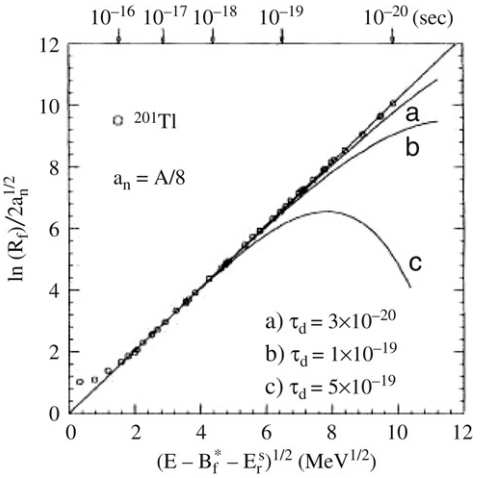

Fig. 26. The quantity $\frac{\ln R_f}{2\sqrt{a_n}}$ versus the square root of the intrinsic excitation energy over the saddle for fission of the compound nucleus ^{201}Tl. The compound nucleus lifetime is indicated on the top. The straight line is a linear fit. The three additional lines represent calculations assuming that no fission occurs during the transient times of 3×10^{-20}, 1×10^{-19} and 5×10^{-19} s. Figure from [85].

has to be noted however that this value of a_f/a_n differs from the a_f/a_n ratios extracted from the previous fitting procedure which may indicate a poorer sensitivity of the data after the scaling procedure as pointed out in [89]. The delaying effect of a possible transient time τ_{trans} – labeled τ_d in Fig. 26 extracted from [85] – on the first chance fission probability, which would deviate from the linear behavior of Fig. 26, has been numerically studied using a step-like time-dependent fission width:

$$\Gamma_f = \Gamma_f^{\infty} \int_0^{\infty} \lambda(t)\ \mathrm{e}^{-t/\tau_{CN}}\,\mathrm{d}t = \Gamma_f^{\infty}\ \mathrm{e}^{-\tau_{\text{trans}}/\tau_{CN}} \tag{8}$$

with

$$\lambda(t) = 0 \quad \text{for } t < \tau_{\text{trans}} \quad \text{and} \quad \lambda(t) = 1 \quad \text{for } t \geqslant \tau_{\text{trans}}. \tag{9}$$

where Γ_f^{∞} denotes the transition state fission width and τ_{CN} is the compound nucleus lifetime. Calculations have been made for several values of transient times and as shown in Fig. 26 no transient delay longer than 3×10^{-20} are found consistent with the scaled data. This approach, following a pure transition state description for fission, is based on expressions valid for first chance fission, dominating the process at low energy and considered by the authors to still account for a large part of the cross sections near the upper energy range. In a comment [89], Back et al. refute the relevance of this hypothesis to derive conclusions on the dynamics of high energy fission. In his reply Moretto shows for ^{211}Po that even a selection of first chance fission does not affect his conclusions.

To study the fission process at high temperature one has to face for nuclei formed in fusion reactions the onset of out-of-equilibrium processes which are difficult to disentangle from complete fusion–fission resulting in wide and quite uncertain distributions of excitation energy, mass, angular momenta... Interesting pieces of information have been brought recently with experiments in which the fissioning nuclei have been produced without compression and with negligible deformational and rotational energies. In these experiments the first steps of the reactions defining the fissioning nucleus properties are described through INC calculations leading to rather well defined initial conditions for fission.

Fission following antiproton annihilation experiments [90,91] have been performed at the low energy antiproton ring LEAR at CERN. Antiproton annihilation allows one to generate high thermal excitation in heavy nuclei with weak distortion related to compression, deformation or angular momentum effects. The heating process in antiproton annihilation reactions occurs through several pions that are emitted in the annihilation. Energy deposition proceeds through their absorption and the excitation of the delta resonance, and thermal equilibrium is reached within less than 10^{-22} s [92], much faster than in the case of heavy ion collisions. This primary step can be modeled with an intranuclear cascade calculation (INC) [93, 94], in which the probabilities of all elementary processes are derived from free meson and baryon interactions. This first step provides thus the characteristics of the transient primary nuclei. Statistical model calculations for their subsequent decay have been performed and then been compared to the observed decay properties, in particular the fission probabilities. Neutrons and charged products, from protons up to fission fragments and heavy residues, were detected over a solid angle of 4π by two concentric spherical detectors. The first one is a silicon ball consisting of 162 modules delivering energy, time-of-flight and pulse-shape discrimination signals for charged species. It was located inside a 4π neutron ball, containing a gadolinium loaded liquid scintillator and measuring the neutron multiplicity on an event-by-event basis. Because of the fast decrease of the neutron detector efficiency with increasing neutron energy, the neutrons arising from the fast INC step are detected with a much lower efficiency than evaporated neutrons. Monte Carlo simulations have shown that the detected cascade neutrons compensate to a large extent for the undetected evaporated ones, on average. Therefore the

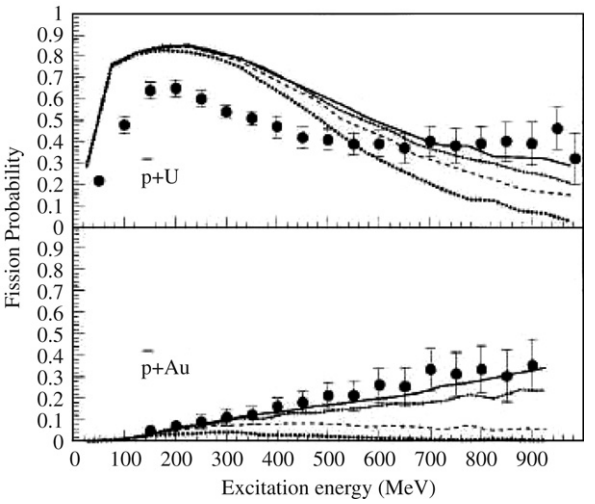

Fig. 27. Experimental fission probability (solid points) plotted as a function of the initial excitation energy of primary nuclei formed in $\bar{p}$ + Au and U. The curves correspond to simulations performed with INC + GEMINI for different transient times : $\tau_{trans} = 0$ (solid), 0.1×10^{-21} s (dot-dashed), 0.5×10^{-21} s (dashed), $2. \times 10^{-21}$ s (dotted). Figure from [91].

measured neutron multiplicity has been identified with the multiplicity of evaporated neutrons. Galilean-invariant velocity distributions have evidenced the evaporative character of the emitted light charged particles. Distributions of excitation energy (E^*) of the transient hot nuclei, extending up to 900 MeV have been determined event-by-event from the total multiplicity of light particles by comparison to the multiplicities predicted by the GEMINI [24] code. GEMINI calculations show that the use of both neutron and charged particles multiplicities allows a much more precise determination of the excitation energy (typically the precision is twice as good) than when only neutrons or charged particles are used. The fission probabilities have then been calculated as a function of the excitation energy and compared in [91] to the predictions of two statistical codes: GEMINI [24] and ABLA [95]. As long as new decay processes such as instantaneous break-up for instance are not open, the fission probability P_{fis} at high excitation energy is sensitive to the transient time necessary for the fission mode to attain its stationary decay width. The increased pre-saddle emission of particles during this transient time leads to decreases in fissility and temperature and thus to a reduction of P_{fis}. This effect is all the more prominent at high E^* as the mean evaporation time becomes shorter. The study of fission probability evolution with excitation energy thus provides information about the fission dynamics prior to the saddle point, as it is insensitive to the further evolution of the nucleus up to scission. In the statistical calculations using GEMINI, the fission width is canceled up to the transient time τ_{trans}, and reaches the Bohr and Wheeler width afterwards. The level density ratio used in the calculations, assumed independent of the energy, has been adjusted on experimental data on fission induced by 1 GeV protons [96]. Comparison between Gemini predictions without any friction and measured fission probabilities are shown in Fig. 27 where the rather large fission probabilities at high excitation energy seem to exclude a transient time τ_{trans} larger than 0.5×10^{-21}.

Alternatively, the measured fission probabilities have been compared in Fig. 28 with ABLA predictions, explicitly considering fission hindrance due to viscosity. Following Grangé et al. [83] a time-dependent fission width has been used with a transient time τ_{trans} given in Eqs. (4) and (5). It has been checked that both GEMINI and ABLA calculations lead to similar results when no friction is considered and the same ratio a_f/a_n of the level density parameters at saddle and ground states are used. For the sake of comparison, the level density parameters have been also taken according to the prescription of Ignatyuk [97] in another calculation with ABLA. With this volume and surface dependency that induces an increase of the level density at saddle as compared to the one at the ground state, experimental fission probabilities at high excitation energy can be as well reproduced by the ABLA code as by the GEMINI calculation for the $\bar{p}$ + U case but are underestimated by a factor of 2-3 for the $\bar{p}$ + Au case. The best agreement is obtained for both targets with a friction coefficient $\beta \approx 3 \times 10^{21}$ s^{-1} corresponding to the shortest possible transient times [84]. This analysis clearly shows that fission probabilities can be reproduced with or without including friction, provided adjustments of the level density parameters are made. However, in any case, the transient times are found to be very short at high excitation energy.

Fission of highly excited nuclei has also been studied using high energy proton- [98] or deuteron-nucleus [99] collisions in reverse kinematics, for which the spallation products are left with low angular momentum and no deformation. Similarly to the $\bar{p}$ induced fission, the reaction has been described as a two step process: a fast interaction between the light particle and the nucleus, described by an INC model (the Liège code [100] for 800 MeV/nucleon Au + p collisions and the Isabel code [101] for the 1 GeV/nucleon U + d collisions), leading to an excited pre-fragment, followed by a slow statistical de-excitation of the pre-fragment. The dynamical evolution of the fission process has been here again, for the 800 MeV/nucleon Au+p collisions, described within the Kramers-Grangé approach Eqs. (1), (4) and (5), using a step-function approximation for the time dependant fission rate whereas, for the 1 GeV/nucleon U + d collisions, the more refined–but leading to similar

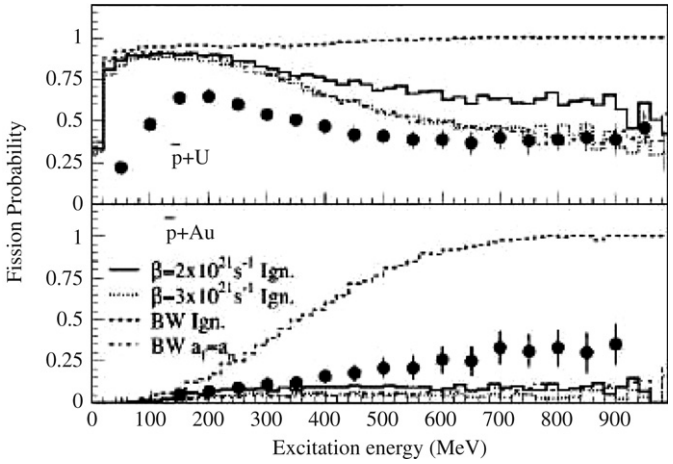

Fig. 28. Same data as in Fig. 27 compared with INC + ABLA calculations for different values of β within the Kramers' approach or within the Bohr and Wheeler approach with different a_f/a_n ratios. Figure from [91].

results–prescription of [61] was used. Reverse kinematics associated with the Fragment Recoil Separator from GSI allow charge and mass identification as well as energy measurement of the emerging fragments.

For the 800 MeV/nucleon Au+p collisions, the atomic numbers Z_{fiss} of the fissioning nuclei were determined from velocity-charge correlations measured for the fission fragments compared with Coulomb repulsion calculations indicating a very narrow range of a few charge units for Z_{fiss}. Fission barriers were taken from Sierk [9] with angular momentum dependence but without additional temperature dependence. Because of similar deformation of saddle and scission configurations in this mass region, the effects of the saddle-to-scission evolution were neglected.

Calculations have been performed with different values of the friction coefficient β and compared with predictions of the standard Bohr and Wheeler approach performed either with a level density parameter ratio $a_f/a_n = 1$ or with the surface and volume dependency of [97]. The calculations made with the Bohr and Wheeler approach underestimated the fission cross-sections for $a_f/a_n = 1$ and overestimated them with the [97] dependence. However, from considerations on excitation energies at the saddle point, the authors exclude this pure statistical description. Excitation energy at saddle has been inferred in [98] assuming a correlation with the width of the fragment charge distribution σ_Z:

$$\sigma_Z^2 = 1/2 \frac{\sqrt{E^*_{B_f}}}{\sqrt{a} C_{\text{mac}}} \tag{10}$$

where $E^*_{B_f}$ is the excitation energy above the barrier, a the level density parameter calculated according to [97] and C_{mac} is the curvature of the macroscopic potential energy at the saddle point as a function of the charge asymmetry obtained from low-energy fission data of pre-actinide nuclei [102]. The validity of this correlation, inspired from the correlation existing at low excitation energies with the mass distribution, has however to be experimentally confirmed. The "experimental" excitation energy inferred with Eq. (10) could only be reproduced with friction dependent fission description with $\beta \approx 3 \times 10^{21}$s. Its value, close to 120 MeV is strongly reduced as compared with the initial excitation energy of the fissioning pre-fragment close to 300 MeV, signing a strong suppression of the fission channel at high excitation energy due to nuclear dissipation. Comparison between calculated and experimental evaporation residues cross sections are displayed in Fig. 29 for a friction coefficient $\beta = 2 \times 10^{21}$ s^{-1}. Very good agreement is obtained except for the residues close to the projectile, a discrepancy interpreted by the authors as a clue for overestimated excitation energies calculated by INC for the most peripheral collisions. This value of the reduced dissipation coefficient $\beta = 2 \times 10^{21}$ s^{-1} corresponds to the shortest transient times $\tau_{\text{trans}} \approx 3 \times 10^{-21}$ s. Calculated mass and charge distributions of the fission fragments also fairly well reproduce the data as demonstrated in Fig. 30 which displays isotopic distributions of fission fragments. The over-prediction for heavy, neutron-deficient fission fragments is once again attributed by the authors to an excess of excitation energy induced in the INC calculation for the most peripheral collisions.

It has to be noted however that very similar experimental results have been obtained earlier for the 1 GeV p+Au system by Andronenko et al. [96] which were interpreted within a pure statistical model without dissipation. The authors of [98] suggest that the discrepancy between the conclusions concerning friction arises from different stiffnesses of the potential used in the calculations implying higher excitation energies at saddle in Andronenko et al. [96] and thus excluding the strong reduction at high excitation energy resulting from a transient delay. As far as the fission probabilities are concerned, it must be stressed however that they are reproduced in Andronenko et al. [96] after an adjustement of the a_f/a_n ratio at a value intermediate to those tested by Benlliure et al. in [98].

In [99] the 1 GeV/nucleon U+d system has been studied with an approach similar to [98]. The INC calculations performed with ISABEL [101] describing the first step of the reaction were tested with projectile residue distributions measured by

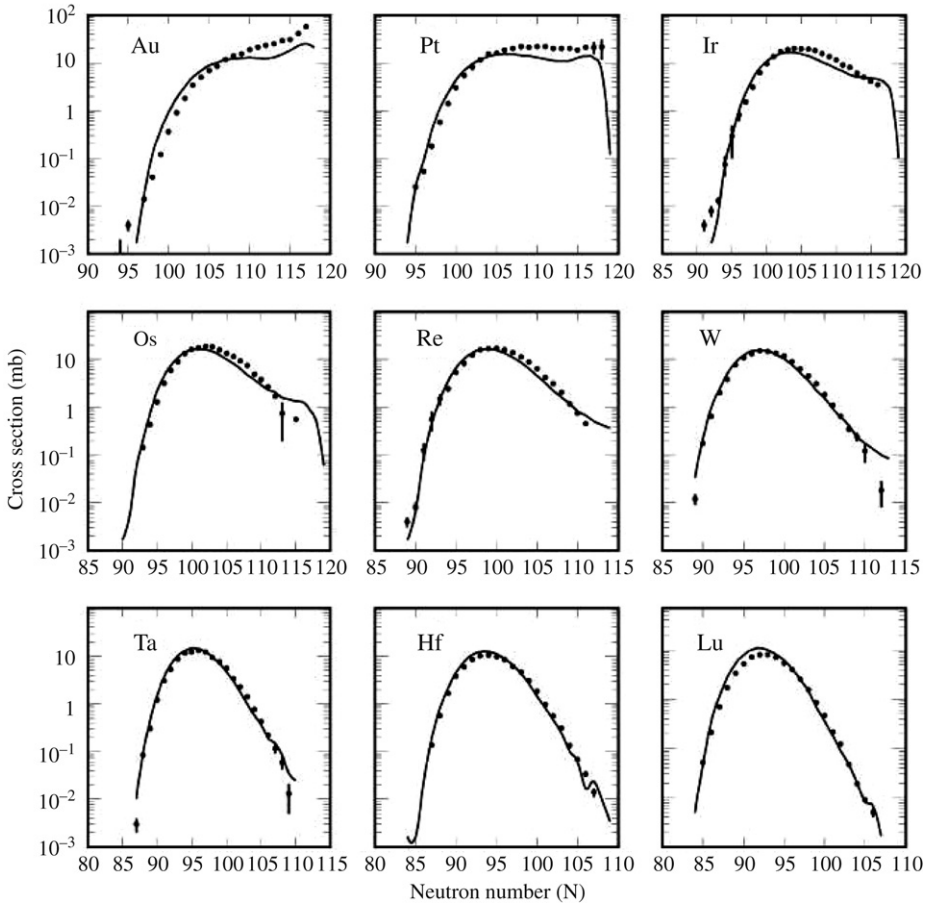

Fig. 29. Measured isotopic distributions of spallation-evaporation residues for elements with an atomic charge larger than 70 produced in the reaction ^{197}Au (800 MeV/nucleon) +p (black dots) compared with simulations made with an INC calculation followed by a Monte Carlo statistical code including a dynamical description of the fission process with a reduced dissipation coefficient $\beta = 2 \times 10^{21}$ s^{-1}. Figure from [98].

Enqvist et al. [103] for the d + ^{208}Pb system at 1 GeV/nucleon in which fission plays a minor role. Considering evaporation residues, the excitation energy predicted by the INC code for the pre-fragment is strongly correlated with the the final mass of the residue, i.e. to the mass loss in the deexcitation stage, as shown in Fig. 31. Such a correlation provides thus an indirect experimental excitation energy scale, which here extends up to much higher values than in the 800 MeV/nucleon Au+p reactions studied in [98]. Therefore the statistical calculations describing the decay step with the ABLA code include a break-up channel which sets in when the temperature exceeds 5 MeV. The experimental residues cross sections for the 1 GeV/nucleon U+d system have been compared to different calculations assuming (i) pure Bohr and Wheeler fission width, (ii) reduced quasi-stationary Kramers fission width without transient, (iii) reduced Kramers fission width with the time-dependent expression of [104]. In every calculation, deformation dependent level density parameter ratios [97] were considered. The best reproduction of experimental cross sections has been obtained for time-dependent fission width with $\beta = 2. \times 10^{21}$ s^{-1}, as in [98]. Nevertheless a quite satisfactory agreement with standard Bohr and Wheeler calculations has been also obtained provided the a_f/a_n ratio is taken equal to unity which were the adopted values in the calculations describing the $\bar{p}$ induced fission of [91] and 2.5 GeV p+U collisions of [105].

Peripheral relativistic heavy-ion collisions have been used in [106,107] to produce highly excited heavy nuclei with small deformation. In [106] Jurado et al. measured fission cross sections and fission fragment charge distributions for 1 GeV/nucleon ^{238}U collisions on $(CH_2)_n$ and lead targets. In [107] Schmitt et al. used fragmentation products of primary 1 GeV/nucleon ^{238}U beam as secondary projectiles impinging at about 530 MeV/nucleon on a lead target. In both experiments, the atomic numbers of the coincident fission fragments were determined in a double ionization chamber. As for such heavy nuclei, the charged particle evaporation prior to scission as well as that originating from the fragments can be neglected, the atomic number of the fissioning system $Z_{\rm fis}$ is simply given by the sum $Z_1 + Z_2$ of the fission fragment atomic numbers. Moreover in abrasion processes $Z_{\rm fis}$ is strongly correlated with the impact parameter of the collision, lower values of $Z_1 + Z_2$ signing smaller impact parameters. The reactions were modeled with the ABRABLA code, describing the abrasion stage followed by the de-excitation stage of the pre-fragment including a fission rate accounting explicitly for viscosity as written in Eq. (1). The fission rate was either considered as constant or as time-dependent, according to the formulation of

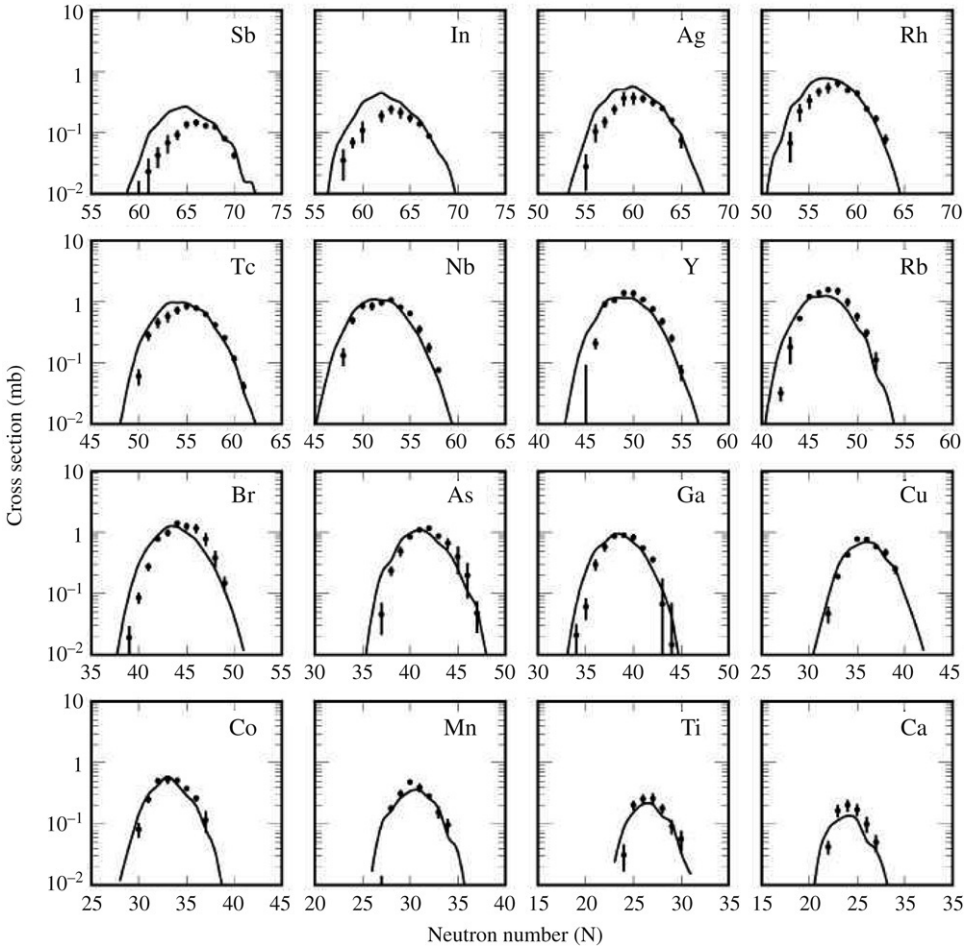

Fig. 30. Measured isotopic distributions of fission residues for selected elements produced in the reaction ^{197}Au (800 MeV/nucleon) +p (black dots) compared with simulations made with an INC calculation followed by a Monte Carlo statistical code including a dynamical description of the fission process with a reduced dissipation coefficient $\beta = 2 \times 10^{21}$ s^{-1}. Figure from [98].

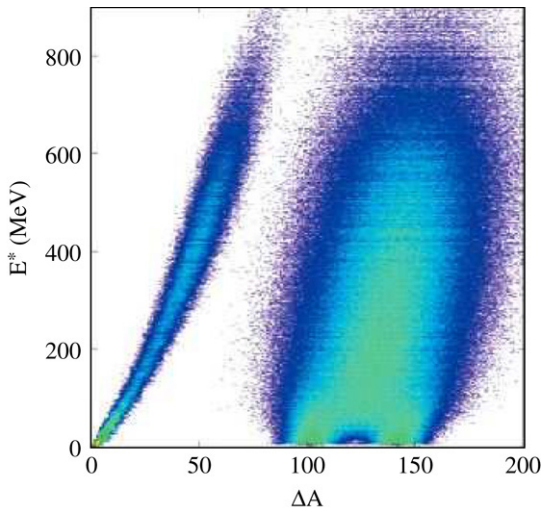

Fig. 31. Excitation energy of the pre-fragment resulting from the intra nuclear cascade as a function of the mass loss of the final residue with respect to the projectile for the reaction ^{238}U (1 GeV/nucleon) + ^{2}H. Figure from [99].

Jurado et al. [61]. A simultaneous break-up process was also considered when the initial temperature of the pre-fragment exceeded 5.5 MeV. By examining the fission cross section as a function of the total charge of the fragments $Z_1 + Z_2$, one expects, in case of large transient times, a strong reduction of the fission probability for the lowest $Z_1 + Z_2$ values due to the short evaporation times associated to the high excitation energies involved. Similarly, by using the assumed linear correlation between the variance σ_A^2 (or σ_Z^2) of the mass (or charge) distribution of the fission fragments [102] and the saddle point temperature (similar to the correlation given in Eq. (10)), the fission hindrance due to transient effects should also be observable on the charge distribution width. An overall agreement between calculated and experimental fission cross sections and charge distribution width is obtained in [106] for $\beta = 2 \times 10^{21}$ s^{-1} corresponding to $\tau_{\text{trans}} \approx 1.7 \times 10^{-21}$s, for the whole range of $Z_1 + Z_2$, giving no evidence for a temperature dependence of the friction coefficient.

In [107] the evolution of the fragment charge distribution width with $Z_1 + Z_2$ has been compared to the ABRABLA calculations for different values of the friction coefficient, for all the 45 secondary spherical beams used. The whole data set is well reproduced with $\beta = (4.5 \pm 0.5) \times 10^{21}$ s^{-1} whatever $Z_1 + Z_2$, i.e. here again without any hint of temperature dependence. The corresponding transient time is $\tau_{\text{trans}} \approx 3.3 \times 10^{-21}$ s. The shorter value of transient time extracted from [106] has been attributed by the authors to the deformation of the fissioning nuclei stemming from fragmentation of prolate ^{238}U projectiles whereas in [107] the initial deformation of the pre-fragment undergoing fission remains small and is of prolate type.

To summarize, concerning the saddle-to-scission times, the recent analyses of pre-scission emission clearly show that the emission during the saddle-to-scission time contributes significantly to the measured multiplicities. Using different assumptions in the analyses of pre-scission particle multiplicity experiments on the evolution with deformation of some essential parameters, this time is found shorter or of the order of 10^{-20} s. This saddle-to-scission time is rather similar to the one inferred from out-equilibrium fission (fast-fission, quasi-fission) [28,32,108,109,30,71], exploring comparable paths in the potential landscape, and of the same order of magnitude than theoretical predictions [110–112].

Important efforts have been devoted to determine from fission probabilities if transient times have to be considered and what would be their effects and magnitude. Fission probabilities have been in particular studied for excited heavy nuclei, produced with low angular momentum and deformation through various reaction mechanisms: $\bar{p}$ annihilation, light particle collisions, peripheral relativistic heavy ion collisions. For all these mechanisms, the primary equilibrium stage is assumed to be very short, with a weak influence on the extracted conclusions, which may not be the case for fusion reactions. It has to be pointed out nevertheless, that the initial conditions for the fissioning nuclei which are used in all the analyses reported here come out most of the times from calculations describing the initial step of the collisions. The above selected examples unambiguously point to the necessity, not yet fully attained, to constrain simultaneously the friction amplitude and the level density parameter ratio a_f/a_n. Two strategies are followed, leading to contradictory conclusions. The GSI group [98,99,106,107] considers explicitly friction with deformation dependent a_f/a_n ratio and friction coefficients close to the critical damping regime are obtained. By contrast the Berlin neutron ball collaboration [90,91,105] analyze the decay of the fissioning excited system within a pure statistical Bohr and Wheeler formalism. Experimental data are reproduced without any friction consideration, provided they use a_f/a_n ratio adjusted on fission or residue cross sections measured at low excitation energies. A further step has been proposed by the GSI group to determine the excitation energy at saddle from the fission fragment mass or charge distribution width to resolve the ambiguity. For instance in [98] no intermediate value between $a_f/a_n = 1$ and $a_f/a_n = 1.05$ can reproduce the extracted value of E^*_{saddle}, even though the fission cross sections may be reproduced with an intermediate value [96]. In that respect, if confirmed, this type of procedure would provide a strong clue for the existence of friction. It must be stressed that when no friction is considered, the data can be reproduced without any transient effect, but transient times up to a few 10^{-22} s cannot be excluded [90,91]. This limit is much shorter than the times inferred for a similar system when friction is taken into account. However, although short, these transient times can be at high excitation energy of the same order or even longer than the *statistical times*. Even if shorter, a significant cooling can occur during this time that must be taken into account for a proper description of the decay process.

5. Conclusion

The different times discussed in this overview should permit a deeper understanding of the fission process and more generally of the dynamical properties of nuclear matter for large scale motion. This perspective has justified important experimental efforts undertaken for more than two decades and still in progress nowadays. We have selected and presented here a few recent and representative papers based essentially on three experimental approaches already described by Hilscher and Rossner in 1992: time measurements through pre-scission multiplicities, through fission probabilities and directly extracted times. These three methods bring complementary pieces of information. They explore different phases of the decay process: pre-scission multiplicities and direct measurements correspond to the evolution up to scission, whereas fission probabilities are only sensitive to the pre-saddle phase. Furthermore, pre-scission multiplicities and direct measurements probe different parts of the scission time distributions, much too broad and complex to be characterized only by their most probable or average values. Direct measurements are sensitive to long scission times whereas pre-scission emission (particles or γ-rays) probes, as shown by Fig. 3, only a shorter part of the scission time distribution. Pre-scission multiplicities are thus strongly dependent on transient effects but an unfolding procedure, giving access to the saddle-to-scission time, has to be applied to separate pre- and post-saddle emission if the latter is significant. Direct

time measurements are sensitive to the fission, particle and γ-ray statistical widths down to the lowest excitation energies and depend thus strongly on the reductions of the fission widths resulting from friction effects.

In contrast to direct measurements, time determination from fission probabilities as well as from pre-scission emission can only be achieved through models. Depending on the considered model, it has been shown that the very same data lead sometimes to quite different extracted time values. Furthermore even within a given model framework, several parameters have counterbalanced effects on fission data (see for instance the discussion ending the previous section concerning the effects of friction and level density parameters), leading to sometimes conflicting conclusions from the very same data.

Strong clues for important friction effects have been found from the three experimental approaches. The long average scission times directly measured for highly excited U-like nuclei can only arise from reductions of the statistical fission widths due to nuclear dissipation. Similarly, friction must be considered for statistical calculations to reproduce pre-scission gamma spectra. On the other hand, fission probabilities may be as well reproduced without friction as with friction, provided different ratios a_f/a_n are used. However the excitation energies at the saddle point are expected to be significantly different in both cases at high initial temperature. Consequently an experimental determination of this excitation energy ought to settle this question conclusively. Attempts have been undertaken to infer this excitation energy from an assumed correlation with the width of fission fragment charge or mass distributions, leading, as with the two other techniques, to the conclusion that friction effects cannot be ignored.

GDR γ-ray spectra measured for different energies point to a dependency of friction amplitude either on temperature or on deformation. Although they cannot exclude a deformation dependency for friction, the direct time measurements dominated by the time spent inside the saddle point, provide strong evidence for a significant increase of friction with temperature.

In most of the analyses, the transient time duration is studied within statistical descriptions of the competition between fission and evaporation despite the obvious conceptual difficulty arising from the dynamical character of this transient period. Even though some recent theoretical approaches express some doubts about a correlation between friction and transient time, all the analyses presented here and including friction effects assume that the friction amplitude defines the transient time. For the other analyses, when friction is disregarded, transient effects are included as a delay related to the finite duration of the shape evolution up to saddle during which fission is hindered (or even canceled). Whatever their assumed origin, the inferred transient times are short, less than or of the order of 10^{-20} s. To get a better insight into transient effects, analyses based on pure dynamical calculations including both evaporation and fission are clearly highly desirable.

Scission time measurements have been recently performed to probe the stability of superheavy nuclei. Fusion processes leading to super-heavy elements that subsequently undergo fission have been identified either from a backtracing procedure applied to neutron data or from long lifetime components evidenced by the blocking technique in single crystals. Since for superheavy elements, the fission barrier heights are governed by shell effects and are essentially experimentally unknown, they can be in principle inferred from fission times. This application to nuclear structure issues opens promising perspectives in the quest for the predicted island(s) of stability and for doubly magic super-heavy nuclei.

Acknowledgements

Many thanks are due to J. D. Frankland for a careful reading of the manuscript.

References

[1] O. Hahn, F. Strassmann, Naturwissenschaften 27 (1939) 11–15.
[2] N. Bohr, J.A. Wheeler, Phys. Rev. 56 (1939) 426.
[3] H.A. Kramers, Physica VII 4 (1940) 284.
[4] Gavron, et al., Phys. Rev. Lett. 47 (1981) 1255–1258.
[5] Gavron, et al., Phys. Rev. Lett. 48 (1982) 835–836.
[6] P. Grangé, L. Jun-Qing, H.A. Weidenmüller, Phys. Rev. C 27 (1983) 2063–2077.
[7] S. Hassani, P. Grangé, Phys. Lett. B 137 (1984) 281.
[8] D. Hilscher, H. Rossner, Ann. Phys. Fratne. 17 (1992) 471.
[9] A. Sierk, Phys. Rev. C 33 (1986) 2039.
[10] I. Gontchar, L. Litnevsky, P. Fröbrich, Comp. Phys. Com. 107 (1997) 223.
[11] P. Fröbrich, I. Gontchar, Phys. Rep. 292 (1998) 191.
[12] K. Pomorski, et al., Nuclear. Phys. A 605 (1996) 87.
[13] I. Gontchar, et al., Yad. Fiz. 63 (2000) 1778.
[14] I. Gontchar, et al., Phys. At. Nucl. 63 (2000) 1688.
[15] V.M. Strutinsky, Phys. Lett. B 47 (1973) 121.
[16] H. Hofmann, F.A. Ivanyuk, Phys. Rev. Lett. 90 (2003) 132701.
[17] H. Weidenmuller, et al., Phys. Rev. C 29 (1984) 879.
[18] M. Morjean, et al., Eur. Phys. J. D 45 (2007) 27.
[19] J. Töke, et al., Nuclear. Phys. A 372 (1981) 141.
[20] Y.A. Lazarev, I.I. Gontchar, N.D. Mavlitov, Phys. Rev. Lett. 70 (1993) 1220.
[21] J. Lestone, et al., Phys. Rev. Lett. 70 (1993) 2245.
[22] S. Cohen, F. Plasil, W. Swiatecki, Ann. Phys. (N.Y.) 82 (1974) 557.
[23] J. Cabrera, et al., Phys. Rev. C 68 (2003) 034613.
[24] R.J. Charity, et al., Nuclear. Phys. A 483 (1988) 371.
[25] A. Gavron, et al., Phys. Lett. B 176 (1986) 312.
[26] K. Siwek-Wilczyńska, et al., Phys. Rev. C 51 (1995) 2054.

[27] K. Ramachandran, et al., Phys. Rev. C 73 (2006) 064609.
[28] R. Butsch, et al., Phys. Rev. C 44 (1991) 1515.
[29] D.J. Hofman, B.B. Back, P. Paul, Phys. Rev. C 51 (1995) 2597.
[30] G. van 't Hof, et al., Phys. Rev. C 54 (1996) R1515.
[31] G. van 't Hof, Nuclear. Phys. A 638 (1998) 613.
[32] I. Diószegi, et al., Phys. Rev. C 61 (2000) 024613.
[33] D.J. Hinde, et al., Phys. Rev. C 45 (1992) 1229.
[34] H. Feldmeier, Rep. Prog. Phys. 50 (1987) 915.
[35] I. Gontchar, M. Morjean, S. Basnary, Europhys. Lett. 57 (2002) 355.
[36] J.U. Andersen, et al., Phys. Rev. Lett. 36 (1976) 1539.
[37] J.S. Forster, et al., Nuclear. Phys. A 464 (1987) 497.
[38] F. Goldenbaum, et al., Phys. Rev. Lett. 82 (1999) 5012.
[39] J.D. Molitoris, et al., Phys. Rev. Lett. 70 (1993) 537.
[40] H.W. Wilschut, V.L. Kravchuk, Nuclear. Phys. A 734 (2004) 156.
[41] M. Morjean, Proc. 3rd Int. Workshop on Nuclear Fission and Fission-Product Spectroscopy, vol. 798, AIP, 2005, p. 194.
[42] D.S. Gemmel, Rev. Modern. Phys. 46 (1974) 129.
[43] S.I. Selem, L.E. Lee, Atom. Data Nucl. Data Tables 18 (1976) 233.
[44] R. Anholt, Rev. Modern. Phys. 57 (1985) 995.
[45] M. Ohta, et al. Proc of Tours Symposium on Nuclear Physics II, 1994, p. 480.
[46] M. Gonin, et al., Phys. Rev. C 42 (1990) 2125.
[47] A.L. Caraley, et al., Phys. Rev. C 62 (2000) 054612.
[48] S. Yamaji, et al., Nuclear. Phys. A 612 (1997) 1.
[49] H. Hofmann, et al., Phys. Rev. C 64 (2001) 054316.
[50] B.B. Back, Phys. Rev. C 60 (1999) 044602.
[51] H. Rossner, et al., Phys. Rev. C 45 (1992) 719.
[52] M. Thoennesen, et al., Phys. Rev. Lett. 59 (1987) 2860.
[53] I. Diószegi, et al., Phys. Rev. C 46 (1992) 627.
[54] K.T. Brinkmann, et al., Phys. Rev. C 50 (1994) 309.
[55] C.R. Morton, et al., Phys. Rev. C 52 (1995) 243.
[56] F. Videbaek, et al., Phys. Rev. C 15 (1977) 954.
[57] B.B. Back, et al., Phys. Rev. C 32 (1985) 195.
[58] F. Pühlhofer, Nuclear. Phys. A 280 (1977) 276.
[59] W. Reisdorf, Z. Phys. A 300 (1981) 227.
[60] S. Shlomo, J.B. Natowitz, Phys. Rev. C 44 (1991) 2878.
[61] B. Jurado, K.H. Schmidt, J. Benlliure, Phys. Lett. B 553 (2002) 186.
[62] P. Møller, et al., Atom. Data Nucl. Data Tables 59 (1995) 185–382.
[63] R. Smolanczuk, Phys. Rev. C 56 (1997) 812.
[64] S. Cwiok, et al., Nuclear. Phys. A 611 (1996) 211.
[65] M. Bender, et al., Phys. Rev. C 60 (1999) 034304.
[66] J.F. Berger, D. Hirata, M. Girod, Acta Phys. Pol. B 34 (2003) 1909.
[67] T. Bürvenich, et al., Phys. Rev. C 69 (2004) 014307.
[68] J. Toke, et al., Nuclear. Phys. A 440 (1985) 327.
[69] W.Q. Shen, et al., Phys. Rev. C 36 (1987) 115.
[70] P.K. Sahu, et al., Phys. Rev. C 72 (2005) 034604.
[71] D.J. Hinde, Nuclear. Phys. A 553 (1993) 255c.
[72] J. Nestler, et al., Phys. Rev. C 51 (1995) 2218.
[73] M.G. Itkis, et al., Nuclear. Phys. A 787 (2007) 150C.
[74] L. Donadille, et al., Nuclear. Phys. A 656 (1999) 259.
[75] T. Materna, et al., Nuclear. Phys. A 734 (2004) 184.
[76] P. Désesquelles, Ann. Phys. Fratne. 20 (1995) 1.
[77] I. Tilquin, et al., Nuclear Instrum. Methods A 365 (1995) 446.
[78] Y. Aritomo, et al., Nuclear. Phys. A 759 (2005) 309.
[79] D. Jacquet, et al., Fusion06, March 19–23 2006 Venezia, Italy, in: Int. Conf. on Reaction Mechanisms and Nuclear Structure at the Coulomb Barrier, vol. 853, AIP, 2006, p. 239.
[80] A. Drouart, et al., Exon04, in: Int. Symp. on Exotic Nuclei, S. World Scientific, PeterHof, 2004, p. 192.
[81] M. Morjean, et al., Phys. Rev. Lett. 101 (2008) 072701.
[82] J. Pouthas, et al., Nuclear Instrum. Methods A 357 (1995) 418.
[83] P. Grangé, et al., Phys. Rev. C 34 (1986) 2063.
[84] K.H. Bhatt, P. Grange, B. Hiller, Phys. Rev. C 33 (1986) 954.
[85] L.G. Moretto, et al., Phys. Rev. Lett. 75 (1995) 4186.
[86] J. Lestone, et al., Nuclear. Phys. A 559 (1993) 277.
[87] C. Cerruti, et al., Nuclear. Phys. A 453 (1986) 175.
[88] J.R. Huizenga, L.G. Moretto, Annu. Rev. Nucl. Sci. 22 (1972) 427.
[89] B. Back, et al., Phys. Rev. Lett. 79 (1997) 4294.
[90] U. Jahnke, et al., Phys. Rev. Lett. 83 (1999) 4959.
[91] B. Lott, et al., Phys. Rev. C 63 (2001) 034616.
[92] J. Cugnon, Nuclear. Phys. A 462 (1987) 751.
[93] J. Cugnon, et al., Ann. Phys. (Paris) 14 (1989) 49.
[94] Y.S. Golubeva, et al., Nuclear. Phys. A 483 (1988) 539.
[95] J. Gaimard, et al., Nuclear. Phys. A 531 (1991) 709.
[96] L. Andronenko, et al., Z. Phys. A 318 (1984) 97.
[97] A. Ignatyuk, G.N. Smirenkin, A.S. Tishin, Yad. Fiz. 21 (1975) 485.
[98] J. Benlliure, et al., Nuclear. Phys. A 700 (2002) 469.
[99] J. Benlliure, et al., Phys. Rev. C 74 (2006) 014609.
[100] J. Cugnon, et al., Nuclear. Phys. A 620 (1997) 475.
[101] Y. Yariv, Z. Fraenkel, Phys. Rev. C 24 (1981) 488.
[102] S. Mulgin, et al., Nuclear. Phys. A 640 (1998) 375.
[103] J. Cugnon, et al., Nuclear. Phys. A 703 (2002) 435.
[104] B. Jurado, et al., Nuclear. Phys. A 757 (2005) 329.
[105] V. Tishchenko, et al., Phys. Rev. Lett. 95 (1985) 162701.
[106] B. Jurado, et al., Phys. Rev. Lett. 93 (2004) 072501.
[107] C. Schmitt, et al., Phys. Rev. Lett. 99 (2007) 042701.
[108] I. Diószegi, et al., Phys. Rev. C 63 (2000) 014611.
[109] N.P. Shaw, et al., Phys. Rev. C 61 (2000) 044612.
[110] H. Hofmann, J.R. Nix, Phys. Lett. B 122 (1983) 117.
[111] Y. Abe, et al., Phys. Rep. 275 (1996) 49.
[112] V. Zagrebaev, W. Greiner, J. Phys. G 31 (2005) 825.